



Regulation of output spike patterns by phasic inhibition in cerebellar granule cells

Thierry R. Nieuws^{1†}, Lisa Mapelli^{2,3†} and Egidio D'Angelo^{2,3*}

¹ Department of Neuroscience Brain Technology, Istituto Italiano di Tecnologia, Genova, Italy

² Neurophysiology Unit, Department of Brain and Behavioral Sciences, University of Pavia, Pavia, Italy

³ Neurophysiology, Brain Connectivity Center, C. Mondino National Neurological Institute, IRCCS, Pavia, Italy

Edited by:

Graziella DiCristo, University of Montreal, Canada

Reviewed by:

Marco Canepari, INSERM, France
Laurens Bosman, Erasmus MC, Netherlands

*Correspondence:

Egidio D'Angelo, Neurophysiology Unit, Department of Brain and Behavioral Sciences, University of Pavia, Via Forlanini 6, Pavia, Italy
e-mail: dangelo@unipv.it

[†]First co-authors.

The complex interplay of multiple molecular mechanisms taking part to synaptic integration is hard to disentangle experimentally. Therefore, we developed a biologically realistic computational model based on the rich set of data characterizing the *cerebellar glomerulus microcircuit*. A specific issue was to determine the relative role of phasic and tonic inhibition in dynamically regulating granule cell firing, which has not been clarified yet. The model comprised the excitatory mossy fiber—granule cell and the inhibitory Golgi cell—granule cell synapses and accounted for vesicular release processes, neurotransmitter diffusion and activation of different receptor subtypes. Phasic inhibition was based on stochastic GABA release and spillover causing activation of two major classes of postsynaptic receptors, $\alpha 1$ and $\alpha 6$, while tonic inhibition was based on steady regulation of a Cl^- leakage. The glomerular microcircuit model was validated against experimental responses to mossy fiber bursts while metabotropic receptors were blocked. Simulations showed that *phasic inhibition* controlled the number of spikes during burst transmission but predicted that it specifically controlled time-related parameters (firing initiation and conclusion and first spike precision) when the relative phase of excitation and inhibition was changed. In all conditions, the overall impact of $\alpha 6$ was larger than that of $\alpha 1$ subunit-containing receptors. However, $\alpha 1$ receptors controlled granule cell responses in a narrow ± 10 ms band while $\alpha 6$ receptors showed broader ± 50 ms tuning. *Tonic inhibition* biased these effects without changing their nature substantially. These simulations imply that phasic inhibitory mechanisms can dynamically regulate output spike patterns, as well as calcium influx and NMDA currents, at the mossy fiber—granule cell relay of cerebellum without the intervention of tonic inhibition.

Keywords: cerebellum, granule cell, GABA-A receptors, synaptic inhibition, modeling, spike timing

INTRODUCTION

Synaptic inhibition controls local microcircuit functions by regulating membrane potential and calcium influx in neurons, with important consequences on spike generation and synaptic plasticity (Llinás et al., 2005; Mann and Paulsen, 2007; Lamsa et al., 2010; Wenner, 2011; Griffen and Maffei, 2014). Since neurons can tune their spike patterns on the millisecond scale (Eccles, 1973; Timmann et al., 1999), it is important to understand how the interplay of excitatory and inhibitory synapses regulates spike timing. Although recent works have raised attention toward the role of tonic inhibitory mechanisms, the role of phasic inhibition was less considered. This reflects the difficulty in dissecting the different components of inhibition pharmacologically and in activating excitatory and inhibitory fibers independently in arbitrary phase relationship.

A prototypical case is posed by the GABAergic inhibitory synapses made by Golgi cells on cerebellar granule cells (Eccles et al., 1964). Granule cells are normally silent at rest and are activated by the mossy fibers. The Golgi cells in turn are activated both by mossy fibers and granule cells (Cesana et al., 2013)

setting up a double feed-back and feed-forward inhibitory circuit. The inhibitory process occurs in the cerebellar glomerulus, a specialized structure enwrapped into a glial sheet, in which several granule cell dendrites are activated by mossy fibers and inhibited by Golgi cells. The limited diffusion space in the glomerulus was shown to favor the establishment of tonic GABA levels and various effects of neurotransmitter spillover and cross-talk (Vos et al., 1999; Forti et al., 2006; Solinas et al., 2007a,b; Kanichay and Silver, 2008). Thus, two inhibitory mechanisms coexist in granule cells. *Tonic inhibition*, which was shown to control the granule spike number (Brickley et al., 1996) and transmission gain (Mitchell and Silver, 2003). *Phasic inhibition*, which was shown to limit the duration of granule cell responses (D'Angelo and De Zeeuw, 2009) and was also implicated in different functions requiring dynamic network control, including generation of granular layer coherent oscillations and resonance (Maex and De Schutter, 1998; Dugué et al., 2009; Solinas et al., 2010; Gandolfi et al., 2013), induction of mossy fiber - granule cell LTP and LTD (Mapelli and D'Angelo, 2007; D'Errico et al., 2009), and spatio-temporal reconfiguration of granular layer activity

(Mitchell and Silver, 2003; Mapelli et al., 2010a). Phasic and tonic inhibition are based on different $\alpha 1$ - and $\alpha 6$ -subunit containing GABA-A receptors and on their differential localization and activation by direct release, spillover and tonic GABA levels (Nusser et al., 1995; Brickley et al., 1996; Rossi and Hamann, 1998; Hamann et al., 2002; Rossi et al., 2003; Farrant and Nusser, 2005; Mapelli et al., 2009, 2014). Although much emphasis has been given to the role of tonic inhibition in regulating granular layer functions, how these mechanisms dynamically regulate granule cell spike patterns has remained largely unexplored. This is somehow surprising for the granular layer, a neuronal micro-circuit which is thought to provide dynamic regulation of spike timing (Eccles, 1973; Fujita, 1982; Timmann et al., 1999).

By exploiting the advanced knowledge on microstructural and molecular properties available, we have modeled the impact of *phasic* and *tonic* GABAergic inhibition on granule cell output spike patterns in response to coactivation of excitatory and inhibitory synapses by a short mossy fiber burst (Pellerin and Lamarre, 1997; Hartmann and Bower, 1998; Chadderton et al., 2004; Rancz et al., 2007; Arenz et al., 2008) and have predicted the impact of single-pulse activation of excitatory and inhibitory synapses with variable phase lag and arbitrary combinations of excitatory and inhibitory synapses (Pellerin and Lamarre, 1997; Hartmann and Bower, 1998; Chadderton et al., 2004; Rancz et al., 2007; Arenz et al., 2008). Model simulations revealed a critical and specific role for phasic inhibitory mechanisms in dynamic regulation of granule cell firing and calcium currents without the need of tonic inhibition.

METHODS

EXPERIMENTAL METHODS

Whole-cell patch-clamp recordings

Patch-clamp recordings in acute cerebellar slices were performed as reported previously (D'Angelo et al., 1995; Armano et al., 2000; Mapelli et al., 2009). Briefly, 17- to 23-day-old Wistar rats were anesthetized with halothane (Aldrich, Milwaukee, WI) and killed by decapitation. Parasagittal 220 μm -thick acute slices were cut from the cerebellar vermis in cold Krebs solution and maintained at 30°C before being transferred to a 2-ml recording chamber mounted on the stage of an upright microscope. The preparations were perfused with Krebs solution (2 ml/min) and maintained at 30°C with a Peltier feedback device (TC-324B, Warner Instruments, Hamden, CT). Krebs solution for slice cutting and recovery contained (in mM): 120 NaCl, 2 KCl, 1.2 MgSO₄, 26 NaHCO₃, 1.2 KH₂PO₄, 2 CaCl₂, and 11 glucose, and was equilibrated with 95% O₂-5% CO₂ (pH 7.4). The patch-clamp pipette solution contained (in mM): 81 Cs₂SO₄, 4 NaCl, 2 MgSO₄, 0.02 CaCl₂, 0.1 BAPTA, 15 glucose, 3 ATP-Mg, 0.1 GTP, and 15 HEPES. For experiments with current-clamp recording the internal solution contained (in mM): 126 potassium gluconate, 4 NaCl, 5 Hepes, 15 glucose, 1 MgSO₄, 0.1 BAPTA-free, 0.05 BAPTA-Ca, 3 Mg²⁺-ATP, 0.1 Na⁺-GTP. These solutions maintained resting free [Ca²⁺] at 100 nM and pH was adjusted to 7.2. Patch-clamp pipettes filled with these solutions had a resistance of 5–8 M Ω before seal formation. Transient current analysis yielded a membrane capacitance (*C_m*) of 3.9 \pm 0.3 pF, membrane resistance (*R_m*)

of 2.0 \pm 0.2 M Ω , and series resistance (*R_s*) of 17.1 \pm 0.9 M Ω (*n* = 7). The 3-dB cell plus electrode cut-off frequency was $f_{VC} = (2\pi R_s C_m)^{-1} = 2.5 \pm 0.1$ kHz (*n* = 7). All drugs were obtained from Sigma, except BAPTA tetrapotassium salt (Molecular Probes, Eugene, OR); GABA-B receptor blockers CGP35348 and CGP55845, mGluRs blockers MCPG, CPPG and gabazine (SR-95531, Tocris-Bioscience). All experiments were conducted in accordance with international guidelines from the European Community Council Directive 86/609/EEC on the ethical use of animals.

Experiments with metabotropic receptors blockers

GABA-B receptor blockers CGP35348 and CGP55845, and the mGluRs blockers CPPG and MCPG were used at 100, 1, 300, and 500 μM , respectively. Perfusion of 10 μM gabazine further blocked the GABA-A receptor mediated inhibition. Incoming mossy fibers were stimulated with 4 pulses at 100 Hz, delivered every 10 s. Initially, no blockers were added to the external solution, the cells were maintained at the holding potential of -65 mV and the granule cells spikes in response to the stimuli were recorded. The same pattern was repeated 30–40 times in control, in presence of metabotropic receptors blockers and after perfusion of gabazine (added to the previous blockers, **Figure 1B**).

Tonic current estimates

The amount of tonic inhibition for each recording was estimated measuring the holding current change ($V_h = -10$ mV) after gabazine perfusion (on average 21.50 \pm 2.12 pA *n* = 6, **Figure 1F**).

Neurotransmission parameter estimates

The specific synaptic organization of the cerebellar glomerulus enables a precise determination of synaptic parameters. EPSCs and IPSCs amplitude, recorded at $V_h = -70$ and -10 mV respectively, was used to estimate the number of excitatory and inhibitory synapses activated by the stimulus. The number of mossy fibers were estimated by the ratio between peak amplitude of EPSCs and single-fiber responses (sfEPSCs) recorded from granule cells in similar experimental conditions (Sola et al., 2004). With an average EPSC amplitude = -81.0 ± 12.9 pA (*n* = 7) and sfEPSC amplitude = -25.8 ± 3.3 pA, the EPSC/sfEPSC amplitude ratio yielded an average of 3.14 activated fibers per granule cell. The number of activated Golgi cell axons was estimated by the ratio between peak amplitude of evoked IPSCs (eIPSC) and spontaneous IPSCs (sIPSC) in the same granule cells. The sIPSCs depend on Golgi cell autorhythmic activity and are generated at single connections (Hamann et al., 2002; Rossi et al., 2003; Mapelli et al., 2009). On average, eIPSCs amplitude was 48.5 \pm 17.8 pA, while sIPSCs amplitude was 16.3 \pm 1.5 pA, so that eIPSC/sIPSC amplitude ration yielded 2.97 GoC axons activated per granule cell (see Mapelli et al., 2009). The parameter space explored in the model was based on the estimates of the number of input contacts (i.e., 1–4 MFs and 0–4 GoC fibers). The comparison between experimental data and model estimates therefore was shown for the 5 granule cells that showed up to 4 GoC and MF inputs (cf. **Figure 1E**, see **Figures 4, 5** and **Table 1**).

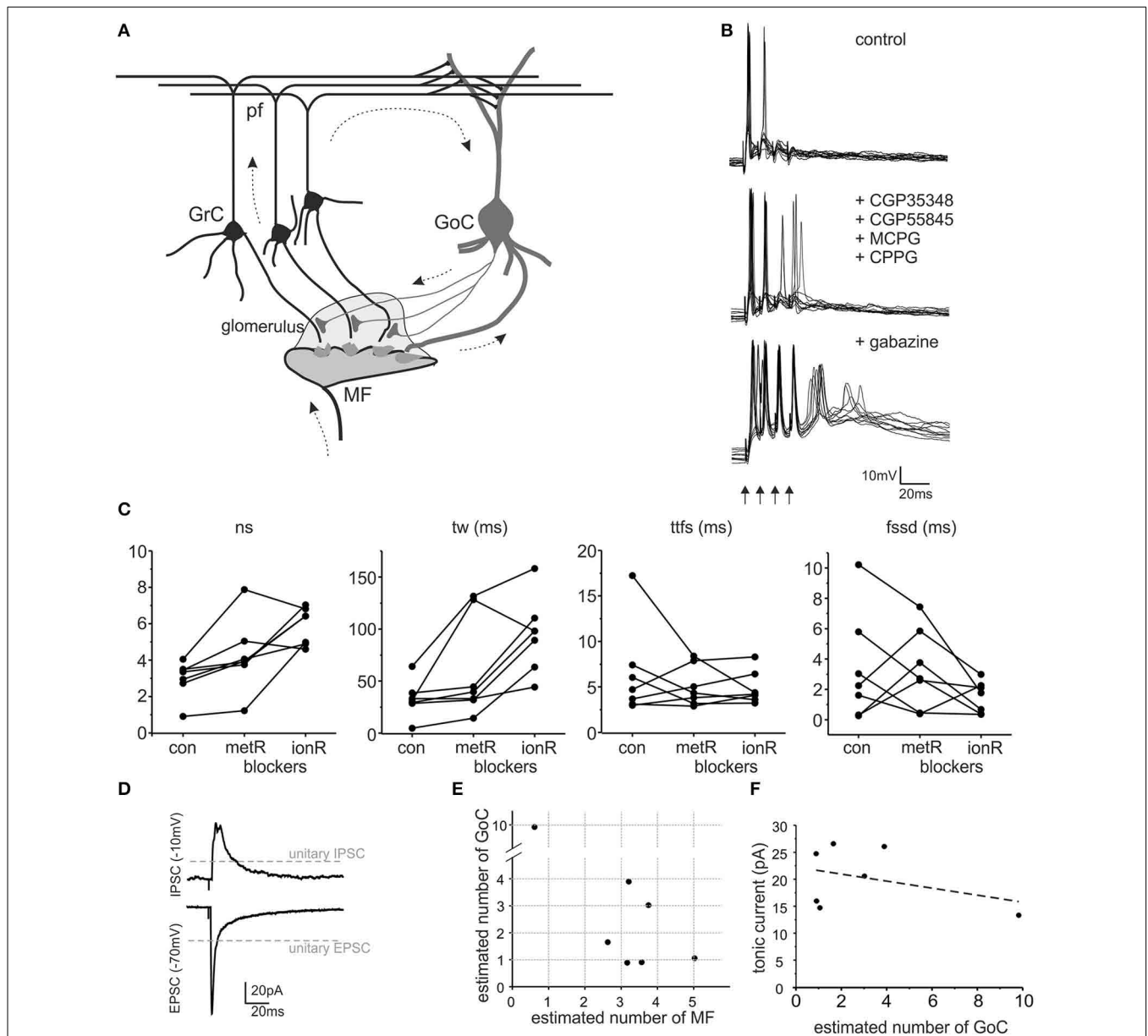


FIGURE 1 | The impact of GABA-A receptors on granule cell excitation.

(A) Schematic drawing of the cerebellar glomerulus. The granular layer of the cerebellar cortex receives input from mossy fibers (MF), making synaptic contacts with granule cells (GrC) and Golgi cells (GoC) in specialized structures called *glomeruli* (light gray area). GrC axons (parallel fibers - pf) contact GoC dendrites. Therefore, GoCs inhibit GrCs through a *feedforward* (MF-GoC-GrC) and a *feedback* (MF-GrC-GoC-GrC) pathway (arrows) (modified from Mapelli et al., 2014). (B) The traces show patch-clamp recordings of GrC activity following a brief burst of MF stimulation (100 Hz, arrows). Glutamatergic and GABAergic metabotropic receptor blockers (MCPG, CPPG, CGP35348, and CGP55845) modify GrC response. The subsequent blockage of ionotropic GABA-A receptors (gabazine) causes an increase in GrC

excitability and spike generation. (C) The plots show the number of spikes (*ns*), time window (*tw*), time to first spike (*ttfs*) and first spike standard deviation (*fssd*) in control (*con*) and after metabotropic receptors blockage (*metR*) and GABAergic ionotropic receptor blockage (*ionR*) in 7 GrC recordings performed as illustrated in (B). (D) Average EPSC and IPSC recorded from the same cell as in (B). (E) The plot reports the estimated number of MF and GoC connections active in each one of the 7 experiments covered in this figure. (F) The plot shows that the tonic current measured after gabazine perfusion in each experiment does not correlate with the number of GoC connections (linear fitting slope -0.65 , $R^2 = 0.137$).

MODELING

In this paper, a computational model of neurotransmission and excitation in the cerebellar glomerulus is developed and a series of routines to investigate the parameter space is implemented.

A single-compartment model of the granule cell [(D'Angelo et al., 2001) updated in Nieuws et al. (2006)] was implemented with advanced representations of inhibitory synapses and run using the NEURON simulator (NEURON version 7.3;

Table 1 | The table summarizes the number of excitatory (n MF) and inhibitory (n GoC) synapses activated during each experimental recording (exp 1–7).

	n MF	n GoC
exp1	3 (3.17)	1 (0.89)
exp2	1 (0.64)	10 (9.82)
exp3	3 (2.63)	2 (1.65)
exp4	4 (3.57)	1 (0.91)
exp5	3 (3.21)	4 (3.90)
exp6	4 (3.75)	3 (3.02)
exp7	5 (5.02)	1 (1.06)

The number of excitatory synapses was estimated by comparing the average amplitude of eEPSCs with the unitary EPSC amplitude (reported in Sola et al., 2004), while the number of inhibitory synapses was estimated by comparing the average eIPSCs amplitude with the sIPSCs amplitude in these same recordings (see Methods). The estimated number of active synapses is indicated in brackets, while the unitary value was used to compare the experimental results to the model.

Hines and Carnevale, 2001). The model was coupled to a recording electrode to reproduce realistic current-clamp conditions and simulations were compared to cellular responses corrected for 10 mV liquid-junction potential. The ionic mechanisms were the same as reported in Nieus et al. (2006) and Solinas et al. (2010). The granule cells are extremely compact also when channels are open in the dendrites during synaptic transmission. Calculations based on cable equation (D'Angelo et al., 1993, 1995; Rossi et al., 1994) and tests using bio-realistic compartmental models (Silver et al., 1992; Diwakar et al., 2009) showed that dendritic electrotonic length was around $L = 0.04$ and the maximum current and membrane potential loss was $<5\%$. Therefore, the results would not be different using single or multi-compartment models.

Major aspects of the inhibitory mechanisms used as the base for modeling

In the cerebellar glomerulus, GABA released from the Golgi cell presynaptic terminal can act directly on receptors facing the postsynaptic site (fast direct component) or indirectly on extrasynaptic receptors through spillover from neighboring sites (slow indirect component) (Rossi and Hamann, 1998; Hamann et al., 2002; Rossi et al., 2003; Mapelli et al., 2009). Direct release from the presynaptic terminal activates $\alpha 1$ GABA-A receptors and, in part, $\alpha 6$ GABA-A receptors. While $\alpha 1$ receptors are located in the PSD, $\alpha 6$ receptors are located preferentially at extrasynaptic sites (but in part also in the PSD, Nusser et al., 1995). Fast kinetics of the direct component are explained by rapid gating of $\alpha 1$ -containing GABA-A receptors. Conversely, slow kinetics of the indirect component are explained by slow gating of $\alpha 6$ receptors largely due to spillover from neighboring contacts (Rossi and Hamann, 1998; Hamann et al., 2002; Rossi et al., 2003). In addition, ambient GABA at sub-micromolar concentration activates high affinity $\alpha 6$ GABA-A receptors generating tonic inhibition.

Mathematical model of inhibitory synaptic transmission

A mathematical model of Golgi cell—granule cell neurotransmission was developed considering available knowledge on the

synapse and on GABA-A receptor kinetics (Cherubini and Conti, 2001; Farrant and Nusser, 2005). The Golgi cell—granule cell IPSCs are generated by different GABA-A receptor subtypes: $\alpha 1$ subunit-containing receptors contribute mainly to early IPSC activation and determine the IPSC peak, while $\alpha 6$ subunit-containing receptors sustain the IPSC along its decay phase (Tia et al., 1996; Rossi and Hamann, 1998; Brickley et al., 2001). Differential receptor activation reflects a range of GABA affinities for the different subtypes. In particular, $\alpha 1$ -subunit containing receptors have EC_{50} in the 10–100 μM range, $\alpha 6\beta 2/3\gamma 2$ receptors have EC_{50} in the μM range, and $\alpha 6\beta 2/3\delta$ receptors have EC_{50} in the 10 nM range (Tia et al., 1996; Nusser et al., 1998; Hadley and Amin, 2007). Differential receptor activation also reflects their subcellular localization. While $\alpha 1$ receptors are localized in the synaptic cleft, $\alpha 6\beta 2/3\delta$ receptors are hundreds of nanometers away from the postsynaptic densities (Nusser et al., 1998), where they are most likely activated by low ambient GABA concentrations and by GABA spillover (10 nM to few μM , (Farrant and Nusser, 2005)). The $\alpha 6\beta 2/3\gamma 2$ receptors are localized in the synaptic junction (Nusser et al., 1998). The simulation of GABAergic neurotransmission in the glomerulus required explicit representations of GABA release and diffusion as well as of the kinetic properties of different GABA receptor subtypes.

Mechanisms of eIPSC generation. GABA release was implemented through a phenomenological 3-state model (ref. Markram and Tsodyks) that well reproduces synaptic dynamics on short time scale, as already demonstrated at the mossy-fiber to granule cell synapse (Nieus et al., 2006). The scheme was governed by recovery rates and release probability from the reserve pool and its output was GABA release. The neurotransmitter concentration, $[GABA]$, was modeled by summing a pulse to a diffusive term:

$$[GABA] = [GABA]_P + [GABA]_D \quad (1)$$

$[GABA]_P$ activates the receptors facing the releasing site, while $[GABA]_D$ accounts for GABA spillover in the glomerulus (Rossi and Hamann, 1998; Nieus et al., 2006). Neurotransmitter concentration at a distance r from the releasing site was described by the diffusion equation:

$$[GABA]_D = \frac{M}{4h\pi D_{eff}} e^{-\frac{r^2}{4D_{eff}t}} \quad (2)$$

where M represents the amount of released neurotransmitter molecules, D_{eff} is the effective diffusion coefficient of GABA molecules, h is the cleft thickness and r is the distance from which the neurotransmitter diffuses. Given the strong similarity of GABA and glutamate molecules (which differ only for a carboxylic group), the diffusion coefficient of GABA was set equal to that of glutamate ($D_{eff} = 0.221 \mu m^2/ms$; Nielsen et al., 2004; Nieus et al., 2006). From morphometry, h was set at 50 nm (Hámori and Somogyi, 1983; Jakab and Hámori, 1988). The parameters M and r in Equation 2 could not be estimated independently and were obtained from fitting (see below and Table 2). To account for the coexistence of direct and indirect components

Table 2 | Model parameters obtained from eIPSC train fittings with the model.

	Control	CGP55845
$G_{max}^{\alpha_1}$ (pS)	1323.25 ± 310.99	
$G_{max}^{\alpha_6}$ (pS)	491.58 ± 112.32	
A (n ^o molec)	10573 ± 3324	
r (μm)	1.07 ± 0.54	
τ_{REC} (ms)	38.7 ± 38.6	
τ_{FAC} (ms)	0	
p	0.42 ± 0.08	0.67 ± 0.09

$G_{max}^{\alpha_1}$ and $G_{max}^{\alpha_6}$ are the maximum conductance of α_1 and α_6 receptors, A is the number of diffusing molecules and r is the diffusion distance, τ_{REC} and τ_{FAC} are the time constants for synaptic vesicle recovery and facilitation, p is release probability. Note that since in all fits the facilitation time constant remained pretty low, τ_{FAC} was fixed to 0 without affecting the quality of the fit itself. The data, except for p , are in common since control and CGP55845 traces were fitted simultaneously and p was the only independent parameter. Data are reported as mean ± s.e.m. ($n = 5$ cells). The model eIPSC train fittings and states are shown in **Figures 2, 3**.

we implemented two separate GABA-A receptor kinetic schemes. The α_1 - and α_6 - receptor responses were reproduced using the same structural kinetic scheme (see **Figure 2A**) while the kinetic rates of the two receptor subtypes were determined by optimization to data taken from the literature (**Figures 2A,B**). The IPSC was then reproduced as:

$$\text{IPSC} = \text{eIPSC}\alpha_1 + \text{eIPSC}\alpha_6 \quad (3)$$

The α_6 component mostly sustains the eIPSC tail after the α_1 response has almost completely decayed (cf. Wall, 2002). Diffusion also contributes to protract the eIPSC through the α_1 component. The GABA channels were given a reversal potential $V_{Cl} = -65$ mV and the tonic component was modeled as a background conductance (D'Angelo et al., 2001).

GABA-A receptor kinetics. The GABA-A receptor models are characterized by two desensitized, three closed and two open states (Barberis et al., 2000; Jones et al., 2001). These models are based on IPSC reconstruction from out-side-out patch-clamp experiments. In whole cell in slices, IPSCs show faster decay than in patches, probably reflecting an increased desensitization caused by phosphorylation of the GABA receptor (Brickley et al., 2001). Interestingly, parallel investigations (Petrini et al., 2011) have demonstrated that the discrepancy between slice and out-side-out experiments might also be determined by the neurotransmitter diffusion in the synaptic cleft that can also shape the IPSC time course.

Recently, a multistate model was proposed that accounts for out-side-out and slice IPSC responses (Pugh and Raman, 2005). The Pugh-Raman model suggests that increasing the transition rate into the fast desensitizing state (“DA2f” in the scheme of **Figure 2A**) can convert out-side-out into slice channel behavior. The α_1 receptor model was obtained by fitting the Pugh-Raman model to sIPSCs generated by the GABA pulse. The α_6 receptor model was obtained by fitting the Pugh-Raman model to slow

eIPSCs activated by GABA spillover (see **Figure 2** in Tia et al., 1996; Rossi and Hamann, 1998; Wall, 2002). Fittings yielded an $EC_{50} \approx 1.5$ μM placing the α_6 -model in the activation range for $\alpha_6\beta_{2/3}\gamma_2$ receptors. Then, α_1 and α_6 receptor currents combined to generate the composite eIPSC. The kinetic rate constants of α_1 and α_6 receptors are reported in **Table 3**.

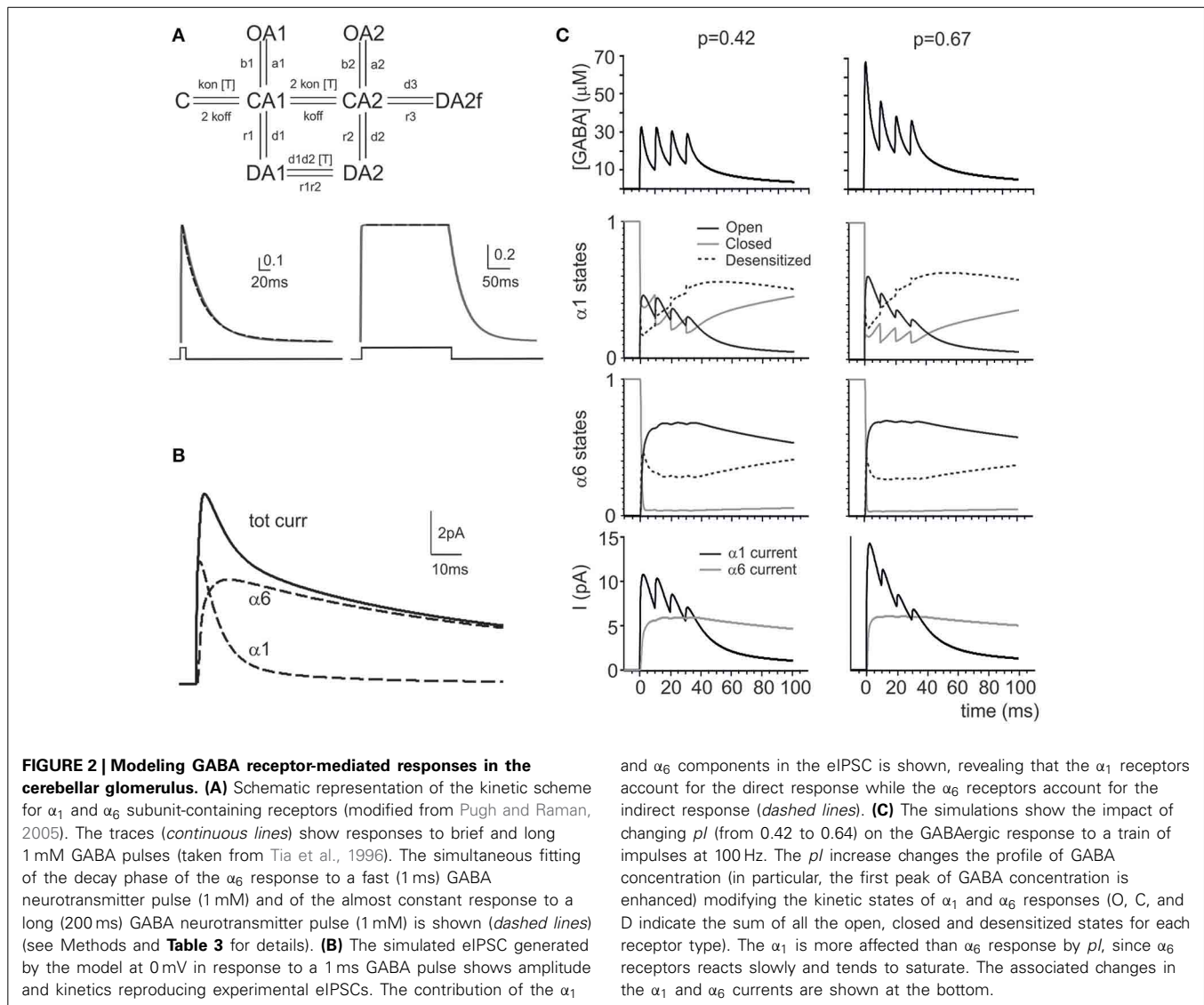
Simulation methods. The model was written in NEURON based on a previous reconstruction of the granule cell (for details see D'Angelo et al., 2001; Nieus et al., 2006) and is available on <http://senselab.med.yale.edu/modeldb/default.asp>. The model allowed to determine neurotransmission parameters through a fitting procedure carried out in two steps. First, single eIPSCs were fitted to determine GABA diffusion parameters (except for h and D_{eff} , which were reported from literature). Then, the whole eIPSC train was fitted on data from our previous experimental investigation (Mapelli et al., 2009) yielding parameters related to synaptic dynamics including the vesicle recycling and facilitation time constants (τ_{REC} and τ_{FAC}) and release probability (p).

Stochastic model. In order to test the GRC responsiveness in a more natural context we introduced synaptic stochastic mechanisms at the excitatory and inhibitory synapses. We modeled stochastic pre-synaptic release of the excitatory and inhibitory phasic components (i.e., the α_1 receptor). The stochastic quantal release model was implemented as in Arleo et al. (2010) by splitting each synapse into a fixed number of independent releasing sites (RS) and independent post synaptic densities (PSD). The presynaptic RSs and the postsynaptic PSDs were endowed with the same kinetic scheme as in the deterministic model. The synaptic conductances were rescaled by the number of RSs. Each stimulus, e.g., presynaptic AP, is broadcast to the RSs and an uniform [0,1] random number (rnd) is generated at each RS where a fixed concentration of neurotransmitter (T_{max}) is released when the corresponding rnd falls below the actual releasable resources (Y). This stochastic model yields the deterministic response when averaged over multiple trials (not shown).

Model of the glomerular microcircuit and simulations

In order to test the responsiveness of the granule cell (GC) in a realistic context, a GC microcircuit was built that included the model of the GC (D'Angelo et al., 2001) as well as its excitatory (Nieus et al., 2006) and inhibitory synapses (developed in this manuscript). At excitatory and inhibitory synapses three independent releasing sites were included (Sola et al., 2004; Mapelli et al., 2009; Arleo et al., 2010), each one comprising the same stochastic release mechanisms. The GC received a maximum of four excitatory mossy fibers (MF) and four inhibitory Golgi (GoC) axons. These average numbers were adopted to limit the parameters space and the case of higher numbers of synapses (e.g., 10 inhibitory synapses in **Figure 1E**) or releasing sites (e.g., see Sola et al., 2004; Saviane and Silver, 2007; Mapelli et al., 2009) were not accounted for.

Two stimulation protocols were used to simulate the impact of the different inhibitory mechanisms on the granule cell output. First, a high frequency input (100 Hz, 4 pulses) was



used to activate the excitatory synapses, while the inhibitory synapses were activated by the same input train delayed by 5 ms to mimic synaptic and integration delays in the feed-forward inhibitory MF-GoC-GC pathway. The results obtained with the first protocol are reported in Figures 4–6. Secondly, single shock stimuli were delivered to the excitatory and inhibitory synapses with a variable phase-lag (from -100 to $+100$ ms). The results obtained with the second protocol are reported in Figures 7, 8.

To the ease of comparison with experimental results we monitored set of parameters such as the number of output spikes (sn), the timing of the first spike (tf_s), the first spike standard deviation ($fssd$, defined as the standard deviation of the measure of tf_s) and the time window of the output spikes (tw , defined as the time difference between the last spike and the first stimulation). Reliable estimates of the measured parameters were then obtained by running 500 runs for each tested condition.

Table 3 | Kinetic rate constants used to simulate α_1 and α_6 GABA-A subunit-containing receptors in cerebellar granule cells.

	α_1	α_6
$k_{on}(\text{mM}^{-1} \cdot \text{ms}^{-1}), k_{off}(\text{ms}^{-1})$	20, 6	54.8, 0.31
$a_1(\text{ms}^{-1}), b_1(\text{ms}^{-1})$	0.06, 0.03	0.06, 0.03
$a_2(\text{ms}^{-1}), b_2(\text{ms}^{-1})$	0.4, 10	0.4, 10
$d_1(\text{ms}^{-1}), r_1(\text{ms}^{-1})$	$3.3e-4, 7e-4$	0.86, 0.04
$d_2(\text{ms}^{-1}), r_2(\text{ms}^{-1})$	1.2, $6e-3$	2.7, 0.43
$d_3(\text{ms}^{-1}), r_3(\text{ms}^{-1})$	15, 3.75	15, 741
$d_1 d_2(\text{mM}^{-1} \cdot \text{ms}^{-1}), r_1 r_2(\text{ms}^{-1})$	15, 0.007	24.2, 0.09

The corresponding simulated traces and kinetic scheme are shown in Figure 2.

Data analysis

All data were analyzed with custom codes developed in Python (www.python.com) based on the Scipy (www.scipy.com), Numpy (www.numpy.com) and Matplotlib (www.matplotlib.com).

com) modules. The analysis allowed to quantify the number of spikes elicited, the time window, the time of the first spike and its variability (i.e., first spike precision) in the tested E/I conditions. In a set of simulations we also recorded the Calcium and NMDA current traces and computed the mean values over a 130 ms long time window.

A compact representation of the E/I space (e.g., **Figure 4B**) was obtained by reporting the excitatory and inhibitory strengths on Cartesian coordinates using a color-code map, in which a color scale corresponded to the intensity of the measured parameter. The excitatory, inhibitory strengths (S_E , S_I) were quantified as the sum of the active fibers (MF/GoC) and their release probability (Pe/Pi), such that $S_E = MF + Pe$ and $S_I = GoC + Pi$.

The $S_{E/I}$ was calculated on sub-regions of the E/I space by averaging over the active fibers involved and the corresponding release probabilities (e.g., **Figure 4B**). Each sub-region was named after the number of active fibers involved: for example, $E/I(1/1)$ corresponds to 1 excitatory and 1 inhibitory fiber. $S_{E/I}$ yields a comprehensive quantification of the changes of the measured quantities at variable E/I levels.

In order to describe the shape of $S_{E/I}$ data distributions at variable phase-lag between synaptic excitation and inhibition, the data were fitted with a Lorentz equation $y(\theta)$ of the form (Gandolfi et al., 2013):

$$y(\theta) = \frac{2 \cdot A}{\pi} \frac{\omega}{4 \cdot (\theta - \theta_{max})^2 + \omega^2} \quad (4)$$

where, A is the underlying area, θ_{max} is the peak frequency, and ω is the width at $y(\theta_{max})/2$. Lorentzian fittings allowed to find the resonance phases ($RF = \theta_{max}$) and to calculate $RA = y(\theta_{max})/\omega$, which corresponds to the quality factor Q in resonance literature and characterizes a resonator's bandwidth relative to its center delay. The goodness of fit was assessed by calculating the squared correlation factor, R^2 . Q is normally used in signal processing theory and describes the tendency of a signal to show resonance vs. monotonic roll-off.

The E/I response space representation also distinguishes between different settings of the GABA tonic current when the phasic component is zero.

Entropy calculation

To estimate the redundancy of the parameters (sn , tw , $ttfs$) on the E/I space we calculated the coding fraction (Borst and Theunissen, 1999; Sadeghi et al., 2007) defined as:

$$CF_P = \frac{MI_P}{H(S)} \quad (5)$$

where $H(S)$ is the entropy of the E/I input space and MI quantifies the mutual information of the measured parameters P ($P = sn$, tw , $ttfs$). Each $S_{E/I}$ configuration of the E/I space was regarded as an independent stimulus. The cardinality of the stimuli is therefore given by: 4 (MF) \times 9 (Pe) \times 5 (GoC) \times 9 (Pi) = 1620. CF_P measures the fraction of $S_{E/I}$ that can be distinguished based on the observation of the whole output generated by the model (i.e., 500 trials for each configuration) and is normalized between

0 (no separation, 100% redundant) and 1 (perfect separation, 0% redundant). CF calculation was performed with the Python module "pyentropy" (Ince et al., 2009) that provides appropriate procedures to robustly estimate MI .

RESULTS

In this paper we have developed a computational model of the cerebellar glomerular microcircuit (**Figure 1A**) and we have simulated its functionality exploring the response space governed by synaptic inhibition. Simulation results were compared with experimental responses to mossy fiber burst stimulation.

THE EFFECT OF INHIBITORY NEUROTRANSMISSION ON GRANULE CELL RESPONSES TO MOSSY FIBER BURSTS

Short high-frequency bursts represent a fundamental pattern of mossy fiber activity (Chadderton et al., 2004). Bursts co-activate granule cells and Golgi cells (D'Angelo et al., 1995; Mapelli et al., 2014). While granule cells depolarization begins, the progressive increase of activity in the inhibitory circuit tends to modulate their response. An early component of inhibition passes through the mossy fiber—Golgi cell—granule cell circuit (feed-forward inhibition), while a late component passes through the mossy fiber—granule cell—Golgi cell—granule cell circuit (feed-back inhibition) (Cesana et al., 2013; D'Angelo et al., 2013).

The impact of inhibitory neurotransmission was investigated by measuring how it modulated granule cell excitation following mossy fiber burst stimulation in acute cerebellar slices (a condition in which feed-forward inhibition prevails). Since metabotropic mechanisms can influence granule cell responses (see (Mapelli et al., 2014) for review), ionotropic effects were isolated using a cocktail of antagonists for mGluRs and GABA-B receptors (CGP35348, CGP55845, MCPG, CPPG) (**Figure 1B**). Following application of these blockers, on average the number of spikes increased (sn change $39.8 \pm 10.5\%$, $p < 0.034$, $n = 7$), the discharge time-window increased (tw change $93.4 \pm 43.1\%$ $p < 0.034$, $n = 7$) while the time-to-first-spike and first spike standard deviation did not vary significantly ($ttfs$ change $-2.3 \pm 17.5\%$, $n = 7$, $p = 0.79$; $fssd$ change $-1.17 \pm 1.34\%$, $n = 7$, $p = 0.97$) (**Figure 1C**). These results show that metabotropic receptors could modify burst transmission to granule cells indicating that the data to be compared to our cerebellar microcircuit model simulations had to be those obtained in the presence of metabotropic receptor blockers.

Inhibitory neurotransmission between Golgi cells and granule cells is mediated by GABA-A receptors, which can be selectively blocked by the GABA-A receptor antagonist, gabazine (Rossi et al., 2003). This receptor antagonist is normally used in a variety of experimental conditions and blocks the phasic and tonic inhibitory processes altogether (Hamann et al., 2002; Nusser and Mody, 2002; Mitchell and Silver, 2003; Rossi et al., 2003; Mapelli et al., 2010a,b; Gandolfi et al., 2013). Following metabotropic receptor blockage (see above), the application of $10 \mu\text{M}$ gabazine significantly increased number of spikes ($68.9 \pm 41.1\%$, $p < 0.05$, $n = 7$) and time window ($112.6 \pm 45.0\%$, $p < 0.04$, $n = 7$) but did not significantly change the time to first spike ($2.74 \pm 10.83\%$, $p < 0.79$, $n = 7$) or first spike standard deviation ($23.4 \pm 80.0\%$, $p < 0.32$, $n = 7$) (**Figure 1C**). Thus, as a whole, GABA-A

receptor-mediated inhibition reduced the intensity and duration of granule cell responses without significantly changing the average time of occurrence and precision of the first spike. This was expected considering that Golgi cell inhibition through the feed-forward circuit usually occurs after the granule cell has emitted the first spike.

In each of the recorded granule cells, measurements of EPSCs and IPSCs were obtained at the reversal potential of IPSCs and EPSCs, respectively (**Figure 1D**). Moreover, the tonic GABA current was estimated by measuring the leakage current before and after gabazine application (not shown). We did not find any significant correlations between the tonic current and the estimated number of active Golgi cell axons (**Figure 1F**), suggesting that the tonic current was regulated by ambient GABA rather than by phasic neurotransmitter release (for review see Mapelli et al., 2014). Specific simulations showed that changes in the tonic current in the range observed experimentally did not significantly affect the model outcome (<5% difference for spike number, first-spike delay, time-window; data not shown). Therefore, in the model tonic inhibition was set as a fixed value, not correlated with the number of active synapses.

The number of active synapses was estimated by comparing EPSCs and IPSCs with the average single-site responses measured previously in identical experimental conditions (**Figure 1D**) (Sola et al., 2004; Mapelli et al., 2009). The estimated number of active mossy fibers ranged from 1 to 5 and that of active Golgi cell synapses ranged from 1 to 10 (**Figure 1E**). Therefore, for each recorded granule cell, the most relevant parameters required to determine its inhibitory control were available and this allowed a direct comparison with simulated data (see **Figure 6**).

MODELING INHIBITORY NEUROTRANSMISSION

A model of cerebellar glomerular inhibition should be able to predict the different kinds of synaptic inhibitory responses observed experimentally in granule cells.

mIPSCs

The minimal GABAergic responses are the miniature synaptic currents, or *mIPSCs*, which correspond to release of single neurotransmitter quanta (Mapelli et al., 2009).

sIPSCs

The spontaneous multiquantal GABAergic responses, or *sIPSCs*, are caused by spontaneous activity in Golgi cells (Dieudonne, 1998; Rossi and Hamann, 1998; Forti et al., 2006; Solinas et al., 2007a,b; Mapelli et al., 2009; Brandalise et al., 2012; Hull and Regehr, 2012). Since *sIPSCs* reflect activation at single Golgi connections, *sIPSCs* are examples of *direct* release without spillover from neighboring contacts.

eIPSCs

The evoked IPSCs elicited by electrical stimulation of the Golgi cell axon, or *eIPSCs* (Rossi and Hamann, 1998; Mapelli et al., 2009), are composed by both a *direct component* due to release of GABA from the presynaptic site facing the postsynaptic density and an *indirect component* due to spillover of neurotransmitter from neighboring presynaptic sites. The decay of *eIPSCs* is indeed slower than that of *sIPSCs*.

Inhibitory synaptic transmission in the cerebellar glomerulus was reconstructed considering the following salient aspects (see Methods for details): (i) the vesicular release cycle contained an explicit representation of the number of releasing sites and of release probability, (ii) the mechanism of vesicle fusion was stochastic, (iii) the postsynaptic membrane expressed α_1 and α_6 receptors, (iv) GABA diffusion was explicitly modeled, and (v) tonic GABA receptor activation was accounted for.

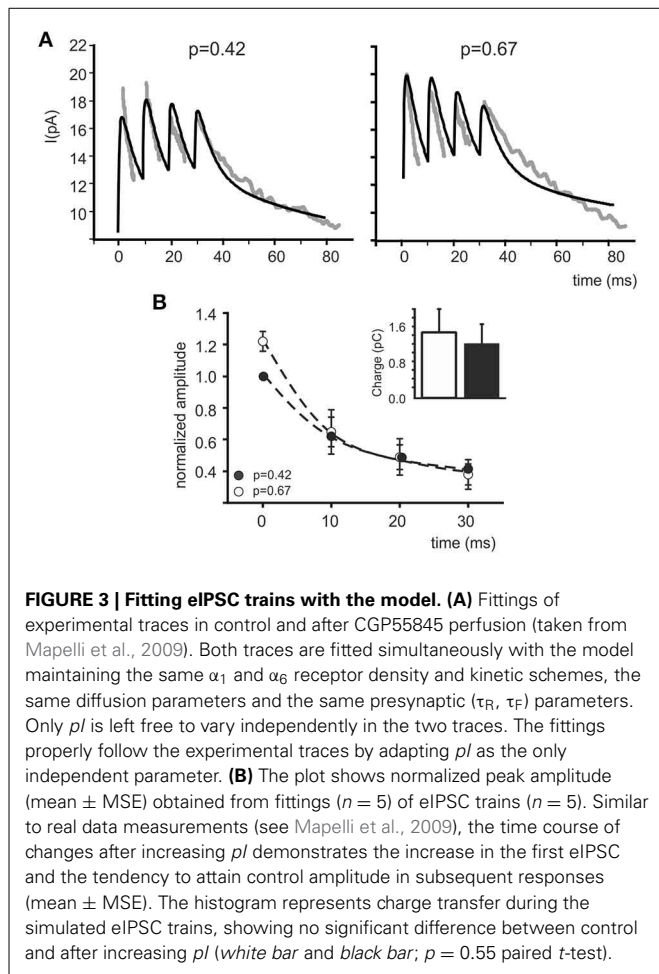
The granule cell GABA receptor models were characterized by two desensitized, three closed and two open states (Barberis et al., 2000; Jones et al., 2001) whose transitions were differentially controlled by GABA transients and slow diffusion waves (Petrini et al., 2011). The GABA receptor responses were modeled using a modified Pugh and Raman (2005) 8-state kinetic scheme using the parameters optimized to match responses generated by GABA pulses (α_1 -type; Brickley et al., 2001) and GABA spillover (α_6 -type; Tia et al., 1996; Rossi and Hamann, 1998; Wall, 2002) (see Methods for details; **Figure 2A**; **Tables 2, 3**). The *eIPSCs* were reconstructed as the sum of α_1 and α_6 receptor-mediated components (**Figure 2B**). The time course of α_1 and α_6 receptor-mediated currents and their combinations were compatible with the time course of *sIPSCs* and *eIPSCs* (Mapelli et al., 2009).

The response of the model during repetitive synaptic transmission is shown in **Figure 2C**. The *eIPSC* peak showed depression along the train, while the *eIPSC* tail showed the marked temporal summation typical of experimental recordings. Clearly, subsequent *IPSC* peaks were driven by oscillations in the activation state of α_1 receptors, while temporal summation was mostly determined by integration of GABA signals through α_6 receptors. The α_6 receptors activated slowly and, due to their high affinity, tended to saturate in a few impulses. Interestingly, changing release probability had a remarkable impact on α_1 receptor-mediated peaks but much less so on the α_6 receptor-mediated current plateau, as further considered below.

MODELING THE EFFECT OF RELEASE PROBABILITY CHANGES

A raise in release probability was proposed to explain the changes in synaptic responses caused by GABA-B receptor blockage by CGP55845 (Mapelli et al., 2009). Here, these changes were simulated by increasing the release probability from $pI = 0.42$ to $pI = 0.67$ (**Figure 2C**). This transiently enhanced GABA concentration in the synaptic cleft, but within 4 impulses the concentration settled toward similar levels with both p values. While the α_1 receptors followed the GABA concentration changes, the α_6 receptors developed similar kinetics at both release probabilities. The slow reaction of α_6 receptors and their early saturation explained the invariance of temporal summation and total charge transfer despite the clear changes caused by pI on the α_1 receptor-mediated response.

In order to test whether a p change could indeed provide a global interpretation of IPSC changes during trains, control and CGP55845 *eIPSC* trains reported by Mapelli et al. (2009) were simultaneously fitted with the model and pI was left free to vary (**Figure 3A**). The fittings yielded $pI = 0.42 \pm 0.12$ in control and $pI = 0.67 \pm 0.13$ in CGP55845 ($n = 5$), in close agreement with experimental determinations ($n = 5$; $p = 0.14$, paired t -test). The



normalized eIPSC amplitude showed a significant difference on the first pulse but then recovered to control values and the total electrical charge transferred during the IPSC train was in good agreement with the experimental one and did not change significantly by raising pI (from 1.19 ± 0.20 to 1.46 ± 0.24 pC; $n = 5$; $p = 0.31$ paired t -test) (Figure 3B). These simulations indicate that a raise in release probability can indeed explain a consistent set of changes in composite α_1 – α_6 receptors-mediated synaptic currents during repetitive neurotransmission suggesting appropriate setting of synaptic transmission parameters.

MODELING THE EFFECT OF INHIBITION ON GRANULE CELL FIRING

In order to quantify granule cell responsiveness in different activation regimens, several series of simulations were run using the *dendritic microcircuit model* (Figure 4A) and the spiking parameters (number of spikes, time-window, time to first spike and first spike standard deviation) were calculated from raster plots and PSTHs of the responses (see Methods). An exhaustive exploration over all possible excitatory/inhibitory (E/I) synapse combinations and release probabilities was performed generating multiparametric color plots (Figure 4B).

Some regularities emerged from this representation. First of all, the parameters varied in a predictable manner with respect

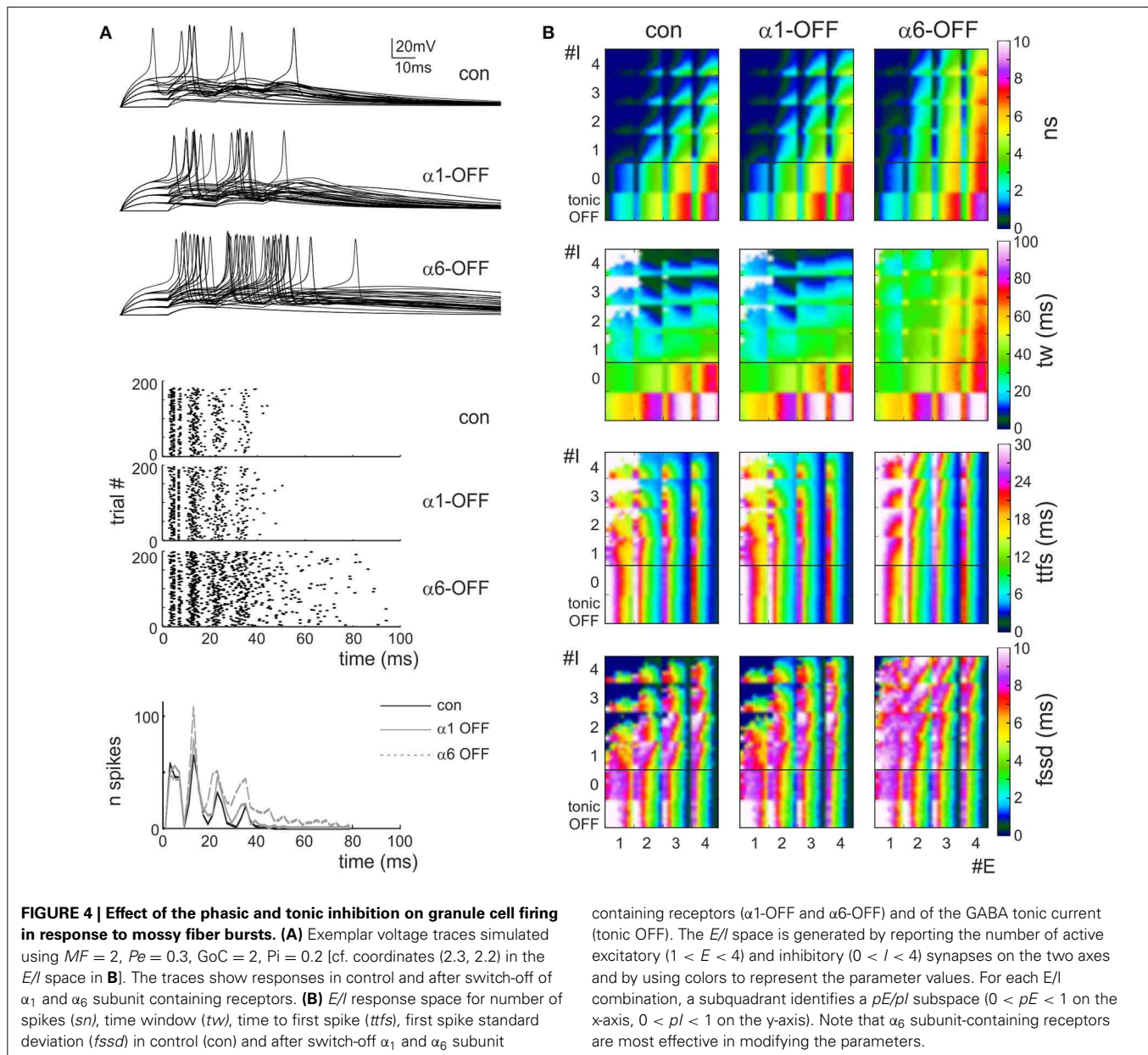
to the E/I balance: number of spikes and time window apparently increased by several times while time to first spike and first spike standard deviation showed modest changes by raising E/I . On a macro-scale, in all graphs an ideal bisectrix separated a low response region (top left, low E/I) from a high response region (bottom right, high E/I). Moreover, a micro-pattern emerged inside each sub-quadrant determined at each E/I by varying excitatory and inhibitory release probabilities, pE/pI . Thus, in principle, by combining different numbers of fibers with different release probabilities, a broad set of response combinations could be obtained generating an extended response space. A quantitative insight on its properties was obtained by considering representative areas. For example, by comparing parameters in the quadrants $E1,2/I3,4$ (low E/I) and $E3,4/I1,2$ (high E/I) there was a nearly 10-fold increase in number of spikes, a 3-fold increase in time window and a modest changes in time to first spike and first spike standard deviation (Figure 5A).

The inspection of the graphs reported in Figure 4B showed that, after switch-off of the phasic components of inhibitory synaptic transmission, number of spikes and time window increased in all quadrants, while time to first spike and first spike standard deviation increased only at low E/I . Interestingly, the effect of α_6 -receptor switch-off dominated over that of α_1 -receptor switch-off in all cases. It should also be noted that the effects of changing E/I and pE/pI , as well as the effects of α_1 and α_6 -receptors switch-off, tuned first-spike timing and precision over the sub-millisecond time-scale and that the spike number varied in discrete units of a few spikes, making the system highly sensitive to activity variations. The complete switch-off of all forms (phasic and tonic) of GABAergic inhibition (simulating a gabazine application see Figure 1) caused a proportionate increase only in spike number and time-window duration without changing time to first spike and first spike standard deviation.

Finally, the model showed that raising pI caused a modest decrease ($\leq 20\%$) of number of spikes, time window, time to first spike and first spike standard deviation. Conversely, raising pE remarkably increased number of spikes ($\leq 80\%$) and decreased time to first spike and first spike standard deviation ($\leq 80\%$) with a limited effect on time window ($\leq 20\%$) (Figure 5B). Therefore, the effect of synaptic inhibition on burst parameters were more related to the number of active inhibitory synapses and to E/I than to the inhibitory release probability.

EXPERIMENTAL DATA IN THE EXCITATORY/INHIBITORY SPACE

The simulated parameters were compared to those measured experimentally (cf. Figure 1). The points were reported in their sub-quadrant following the indications derived from Figure 1E and located at the corresponding pE/pI intersection (Figure 6A). In this comparison we used only the 5 granule cells with $E, I = 4$ in order to fit into the simulated parameter space. For these cells, the pE and pI values closely corresponded to those reported previously (Sola et al., 2004; Mapelli et al., 2009) (Figure 6B). The parameter variation caused by gabazine was then compared to that caused by switch-off of both tonic and phasic synaptic inhibition in the model (Figure 6C). The data measured for the different parameters showed a variation similar to that of the



model (linear fitting with slope 0.95, $R^2 = 0.914$). It should be noted that this data distribution was not significantly different from the unitary diagonal ($X^2 p < 2.6 e^{-10}$). Finally, it should be noted that time to first spike and first spike standard deviation showed modest changes compared to number of spikes and time window, in agreement with experimental results matched for the E/I balance (experimental $E/I = 2.2$ compared to simulated $E/I = 2.6$). Therefore, the model was able to capture the main quantitative properties of glomerular transmission and the impact of synaptic inhibition on granule cell firing.

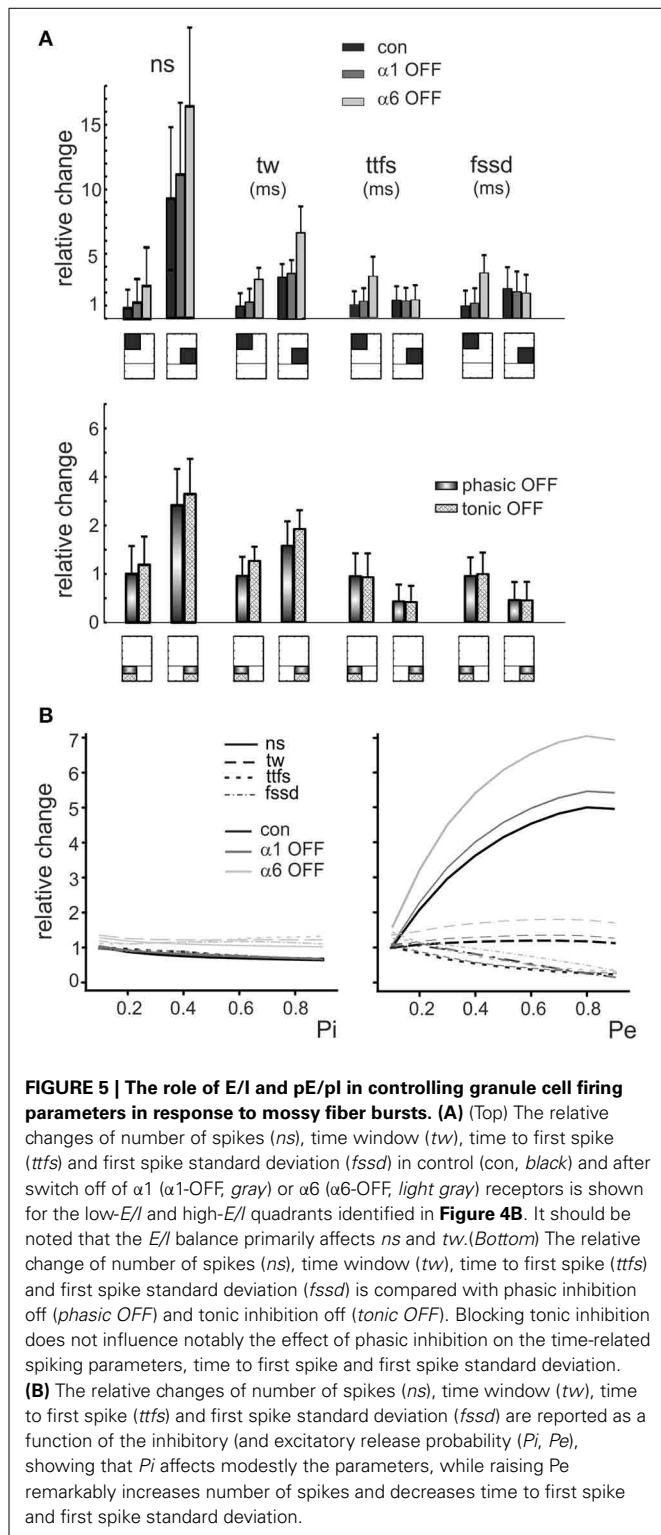
INFORMATION CODING IN THE EXCITATORY/INHIBITORY SPACE

In order to assess the impact of inhibition on information coding (i.e., to what extent the same responses could be obtained with different parameters), the coding fraction (actually the ratio

between mutual information and entropy, see Methods) was calculated (Borst and Theunissen, 1999; Sadeghi et al., 2007; Ince et al., 2009). The coding fraction of number of spikes, time window, and time to first spike was relatively small (see **Table 4**) demonstrating a remarkable redundancy in the parameter space. Once inhibition was removed by blocking α_1 and α_6 receptors, the coding fraction increased for time window and time to first spike, but not apparently so for the number of spikes (**Table 4**), indicating a preferential control of inhibition over spike patterning and timing rather than on spike number *per se*.

THE IMPACT OF E/I PHASE ON SPIKE GENERATION AND ON NMDA AND VDCC CURRENTS

Beside the coordinated action of excitation and inhibition caused by concurrent mossy fiber activation of granule cells and Golgi



cells shown in Figure 4, the excitatory and inhibitory synapses impinging on granule cells can work in any arbitrary phase relationship. Given their different time-course and temporal integration during trains (cf. Figures 2, 3), $\alpha 1$ and $\alpha 6$ receptor-mediated currents might have differential impact on firing depending on

the *E/I* phase (Figure 7A). Therefore, we have performed simulations using different phase-lags of inhibition with respect to excitation generating *tuning curves* for the spiking parameters (in these simulations *pE* and *pI* were not changed since we used single stimulation pulses preventing their impact on short-term train dynamics). The most apparent changes occurred when $\alpha 6$ receptors were switched off. Interestingly, number of spikes, time window, time to first spike and first spike standard deviation showed resonance around -10 ms phase-lag. When $\alpha 1$ receptors were switched off, resonance appeared around 10 ms phase-lag. The impact of the *E/I* phase was evaluated also for currents generated by NMDA channels and voltage-dependent calcium channels (VDCCs) (Figure 7B). Again, the most apparent changes occurred when the $\alpha 6$ receptor was turned off. The VDCC current decreased monotonically with positive phase-lag while the NMDA current showed broad tuning distributed between -20 and $+30$ ms phase-lag. When the $\alpha 1$ receptor was turned off, resonance peaked around $+10$ ms phase-lag.

These simulations showed that $\alpha 1$ and $\alpha 6$ receptor-mediated effects combined in tuning spike generation toward specific phase-lags and that $\alpha 6$ receptor-mediated effects were larger and broader than $\alpha 1$ receptor-mediated effects.

MODULATION OF TUNING CURVES BY THE E/I PHASE AND TONIC INHIBITION

The tuning curves reported in Figure 7 revealed dependence of granule cell responses on the *E/I* phase-lag. This effect was evaluated by fitting the tuning curves with Lorentzian functions yielding $Q = A/\omega$, a parameter indicating the tendency of the response to peak at a certain phase-lag θ_{max} with area *A* and broadness ω (Equation 4, see Methods; Figure 8A).

Lorentzian parameters, which report the effectiveness of tuning toward a preferential phase-lag, showed specific properties (Figure 8B). For all parameters, $Q(\alpha 6) > Q(\alpha 1)$ reflected the larger impact of $\alpha 6$ than $\alpha 1$ receptor-mediated charge transfer, $\omega(\alpha 6) > \omega(\alpha 1)$ reflected the longer duration of $\alpha 6$ than $\alpha 1$ receptor-mediated responses, and $\theta_{max}(\alpha 6) < 0$ and $\theta_{max}(\alpha 1) > 0$ reflected the slower raise of $\alpha 6$ than $\alpha 1$ receptor-mediated responses (cf. Figures 2, 3). Interestingly, $Q(\alpha 6)$ was much larger for time window, time to first spike and first spike standard deviation than for number of spikes (Figure 8B). This pattern was opposite to that observed for burst transmission (cf. Figure 5A), implying that only the time-dependent parameters were tuned by the *E/I* phase difference. It should also be noted that $Q(\alpha 6)$ of the NMDA current was very small, reflecting the slow time course of this current and its broad integration times (D'Angelo et al., 1995; Schwartz et al., 2012).

Modulation of $Q(\alpha 6)$ for time window, time to first spike and first spike standard deviation tended to decrease with *E/I*, according to the powerful effect of phasic inhibition in controlling time-dependent parameters (Figure 8C). Modulation of $Q(\alpha 6)$ with *E/I* for the VDCC current followed strictly that of the number of spikes (D'Angelo et al., 1999; Gandolfi et al., 2014). Modulation of $Q(\alpha 6)$ with *E/I* for the NMDA current was marginal but, specifically, $\theta_{max}(\alpha 6)$ shifted progressively from -20 to $+30$ ms (phase-lag precession, cf. Figure 7B) with increasing *E/I* (Figure 8D)

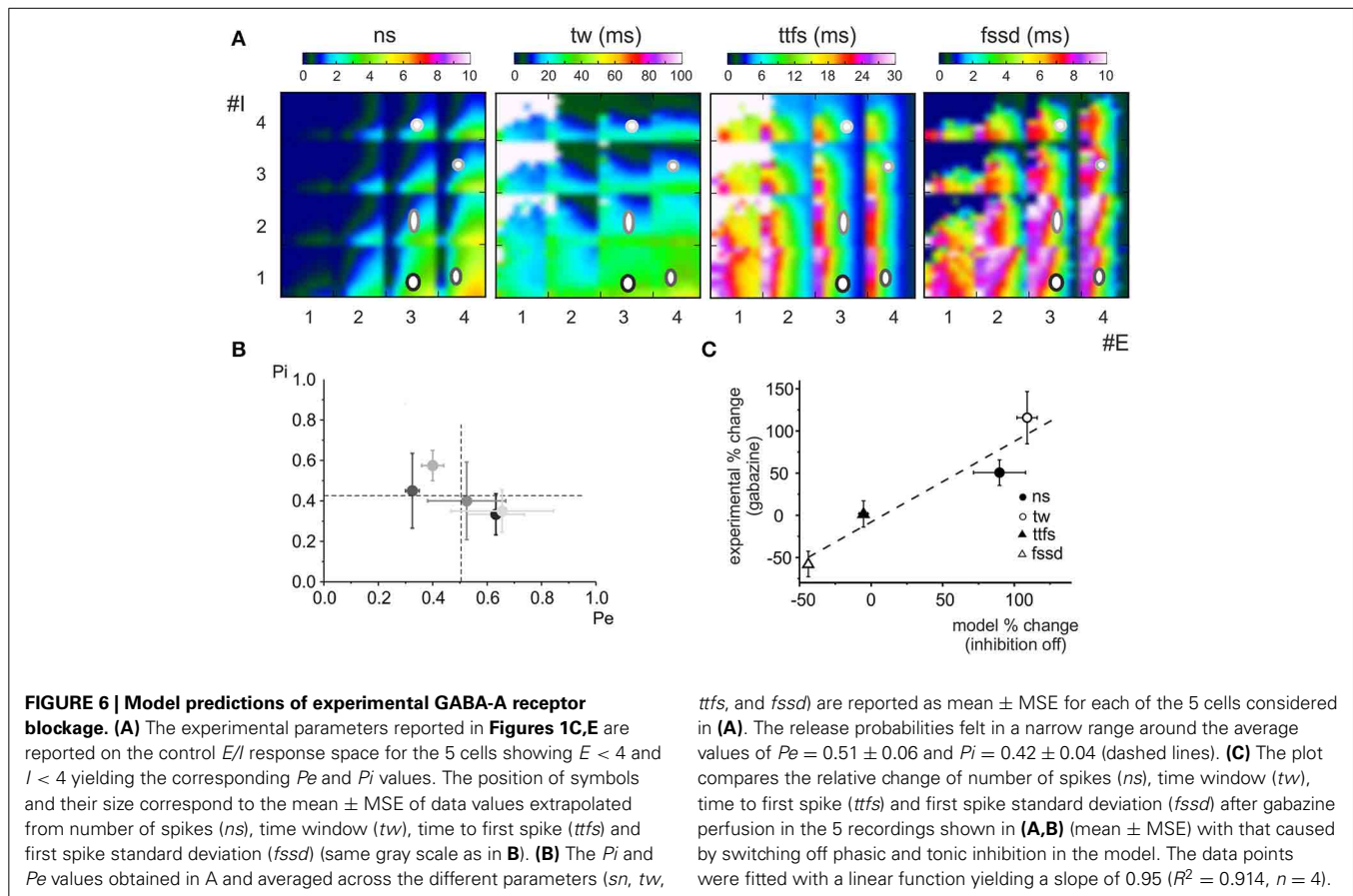


Table 4 | Coding fraction of number of spikes (*sn*), time window (*tw*) and time to first spike (*ttfs*) was relatively small demonstrating a remarkable redundancy in the parameter space.

	<i>sn</i>	<i>tw</i>	<i>ttfs</i>
CTRL	0.123	0.144	0.192
$\alpha 1$ OFF	0.128	0.165	0.211
$\alpha 6$ OFF	0.121	0.181	0.233

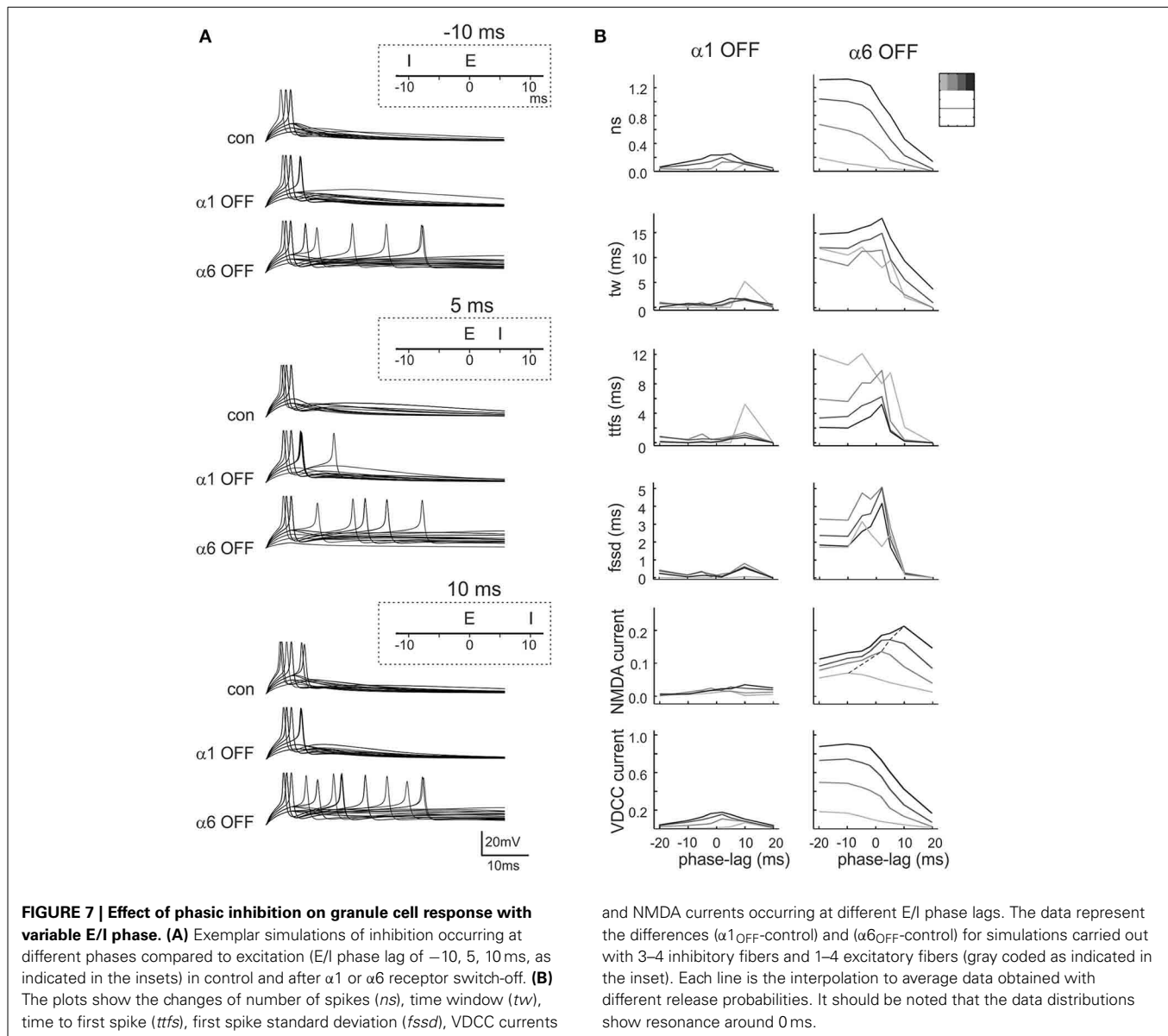
Once inhibition was removed by blocking $\alpha 1$ and $\alpha 6$ subunit-containing receptors, the coding fraction increased for time window and time to first spike, but not apparently so for the number of spikes, indicating a preferential control of inhibition over spike patterning and timing rather than on spike number per se.

unveiling a complex influence of $\alpha 6$ receptor-mediated inhibition on voltage-dependent NMDA channel unblock.

Finally, in order to determine the effect of tonic inhibition on granule cell responses to dynamic patterns, tuning curves were generated with tonic inhibition blocked. The plot in Figure 8C shows the difference between the cases in which tonic inhibition was on or off. The tonic current biased the effect of inhibition proportionately to the *E/I* balance without altering the dynamics of inhibition substantially. Therefore, the model predicts that tonic inhibition simply scales the effect of phasic inhibition on firing parameters.

DISCUSSION

In this paper we have developed a detailed *glomerular microcircuit model* in order to assess how phasic and tonic components of GABA-A receptor-mediated inhibitory neurotransmission contribute to dynamic regulation of firing in cerebellar granule cells. The main prediction of this model is that *phasic inhibition* can dynamically regulate granule cell firing in response to temporally organized patterns of mossy fiber and Golgi cell activity. Phasic inhibition preferentially controlled the number of spikes during transmission of short bursts, but it showed improved control over time-related parameters (time to first spike, first spike standard deviation and time window) when the *E/I* phase was changed. In all conditions, the overall impact of $\alpha 6$ was larger than that of $\alpha 1$ subunit-containing receptors. However, $\alpha 1$ receptors controlled granule cell responses in a narrow ± 10 ms band while $\alpha 6$ receptors showed broader ± 50 ms tuning. Eventually, phasic inhibition fine-tuned the initiation and termination of granule cell firing during burst-burst transmission, as well as the probability of firing at different *E/I* phases, on the millisecond-scale. The model also predicts that *tonic inhibition* can bias these effects without changing their nature substantially. These results imply that the specific organization of phasic inhibitory mechanisms can effectively regulate the dynamics of spike generation at the mossy fiber - granule cell relay of cerebellum without the intervention of tonic inhibition.



THE PREDICTIVE POWER OF THE GLOMERULAR MICROCIRCUIT MODEL

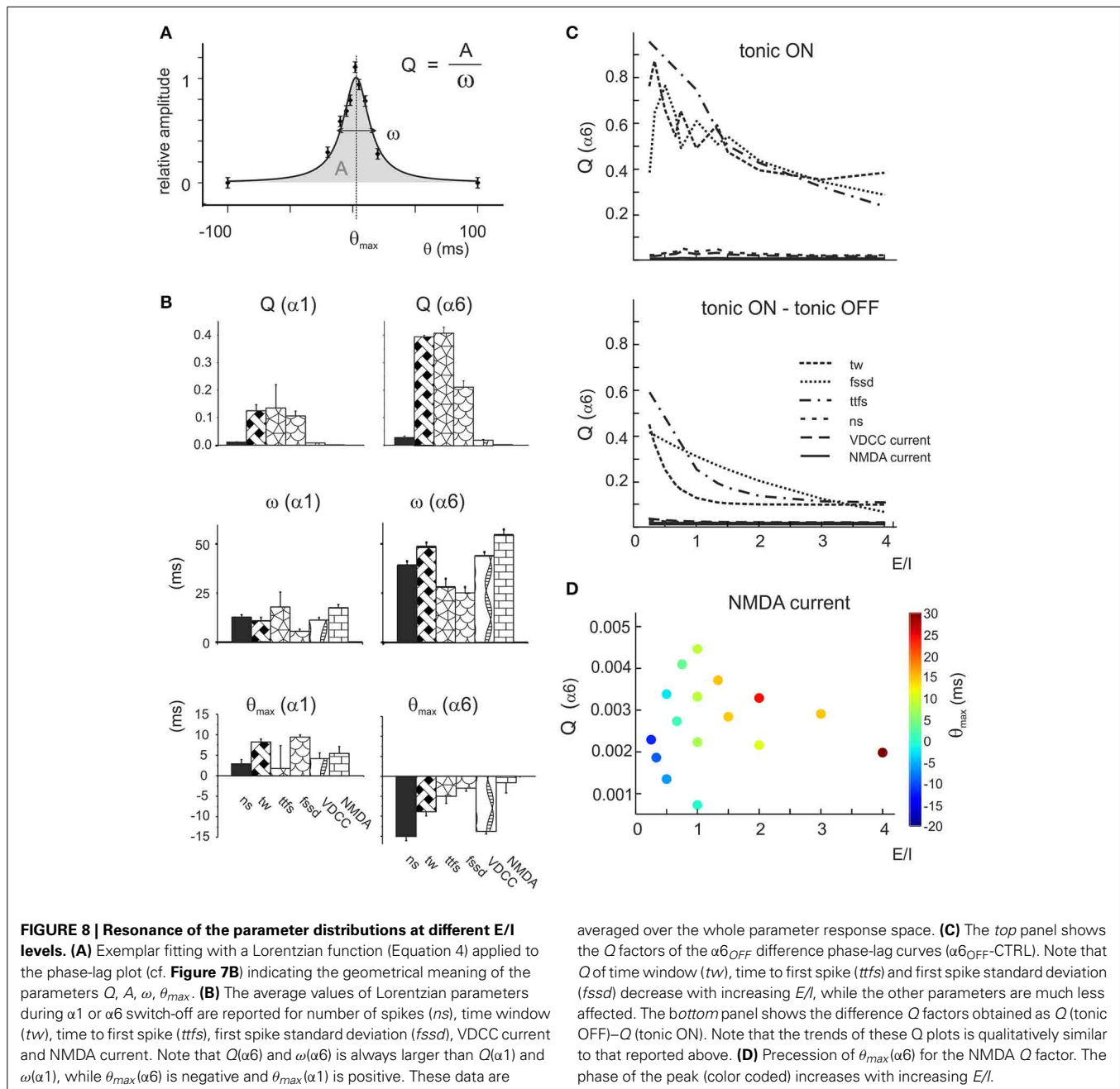
The *glomerular microcircuit model* could fit and explain the firing patterns observed in experimental data following mossy fiber burst stimulation. Once experimental granule cell firing parameter (time to first spike, first spike standard deviation, number of spikes and time window) values were reported on the simulated response space, the *glomerular microcircuit model* yielded *pE* and *pI* values corresponding to those observed experimentally (average *pE* = 0.51 vs. 0.55 in (Sola et al., 2004); average *pI* = 0.42 vs. 0.42 in Mapelli et al., 2009). Moreover, the model properly fitted the spiking parameters changes caused by gabazine, a drug that blocks both phasic and tonic inhibition. Therefore the model was endowed with mechanisms capable of capturing the impact of inhibitory neurotransmission on granule cell firing parameters and could be used to predict the effect of different E/I phase lags.

It should be noted that in our model the effect of metabotropic receptors was excluded to isolate the ionotropic component

of inhibition. Experimentally, the application of mGluRs and GABA-B receptor blockers caused a net disinhibitory effect (cf. **Figure 1**), which could reflect multiple mechanisms. The mGluRs on presynaptic Golgi cell terminals might have reduced GABA release, and this would suffice to explain the increased number of spikes and duration of discharge in most of the recordings. Conversely, GABA-B receptor blockage on granule cells and on Golgi cell terminals (Rossi et al., 2006; Mapelli et al., 2009) would reduce granule cell excitability and enhance inhibitory neurotransmission, thereby sorting the opposite effect. Future models of glomerula neurotransmission may be designed to include metabotropic receptor control (Mapelli et al., 2014).

PROPERTIES OF THE INHIBITORY NEUROTRANSMISSION MODEL

The inhibitory neurotransmission model was based on GABA-A receptor kinetics and was fitted to voltage-clamp recordings. Simulations of glomerular inhibition were consistent with a



mechanism in which α_1 receptors determine the rapid response to released GABA characterizing the direct component, while α_6 receptors determine the slow temporal integration of spillover currents characterizing the indirect component (Cherubini and Conti, 2001; Farrant and Nusser, 2005; Glykys and Mody, 2007). The model predicts that, while α_1 receptor-mediated responses can precisely follow GABA concentration changes, α_6 receptor-mediated responses tend to saturate early during the train. Thus, as observed experimentally, raise in p determined minor changes in synaptic charge transfer matching experimental observations (Mapelli et al., 2009).

The adherence of the inhibitory neurotransmission model to the microscopic properties of the synapse could be defined

at different levels. First, the GABA-A receptor kinetic schemes (derived from Pugh and Raman, 2005) appropriately reproduced eIPSCs and their changes in different functional conditions, suggesting that GABA affinities and the balance between open, closed and desensitized states were in the physiological range for granule cell receptors. Secondly, by setting the same diffusion coefficient for GABA and glutamate (DiGregorio et al., 2002), the number of diffusing molecules and the diffusion distance were similar to those estimated for the mossy fiber—granule cell synapse (Nieuws et al., 2006). This was not unexpected, given the substantial similarity in the number of releasing sites involved and the common diffusion space for the two neurotransmitters. Thirdly, the p values obtained by fitting the model to experimental data were

almost identical to those estimated experimentally with quantal analysis and no changes in the rate of vesicle recycling or in any other model parameters were needed to fit the experimental eIPSC trains.

INHIBITORY CONTROL OF GRANULE CELL FIRING DURING BURST TRANSMISSION

Model simulations explained the complex effect of phasic inhibition on the burst-burst transmission modality of the granular layer (Chadderton et al., 2004; Rancz et al., 2007; Arenz et al., 2008). The E/I balance was most effective in controlling granule cell tonic discharge (the ~ 9 -fold number of spikes increase was associated with a ~ 3 -fold time window increase, so that the output spike frequency increased by about 3 times) but had minor effects on time-related parameters, time to first spike and first spike standard deviation. The pE/pI balance was most effective in controlling number of spikes, time to first spike and first spike standard deviation. Raising pE specifically increased number of spikes and reduced time to first spike, consistent with the fact that AMPA and NMDA receptor activation shows a remarkable modulation with pE (Nieus et al., 2006). Raising pI depressed all parameters but its effect was small, probably because inhibition during a burst largely depends on the charge carried by $\alpha 6$ receptors, which are early saturated (see above and cf. **Figures 2, 3**). The first spike standard deviation was almost equally reduced by raising pE and pI , probably reflecting reduction of synaptic noise determined by the larger number of released quanta (Sola et al., 2004; Mapelli et al., 2009). It turns out that, during burst transmission, the major effect of inhibition is to control the number and frequency of spikes emitted by granule cells through a regulation of the relative number of active Golgi cell synapses. Both E/I and pE/pI effects were enhanced by GABA receptor switch-off, but the contribution of $\alpha 6$ was always much larger than that of $\alpha 1$ receptors reflecting the fact that $\alpha 6$ receptors controlled most of the inhibitory charge transfer.

The tonic GABA leakage in the model did not contribute to the effect of inhibitory transmission substantially beside proportionately increasing number of spikes and time window. The tonic GABA leakage was modeled on the basis of experimental observations in cerebellar slices. The cerebellar glomerulus is an ideal structure to preserve tonic inhibition in slices provided that the glial sheath is intact (Hamann et al., 2002; Mitchell and Silver, 2003; Mapelli et al., 2014). Although the topic is still debated, tonic inhibition was reported *in vivo* revealing properties similar as in slices (Chadderton et al., 2004), suggesting that predictions made by our model could apply to synaptic transmission in natural conditions.

INHIBITORY CONTROL OF GRANULE CELL FIRING WITH VARIABLE E/I PHASE

Model simulations predicted a specific role for phasic inhibition in controlling granule cell responses with different E/I phases lags. The most apparent regulatory effects on granule cell firing occurred when the $\alpha 6$ receptor-mediated current was turned off. This was due to the long time course and large charge transfer of $\alpha 6$ receptor-mediated responses, extending the influence of inhibition for about ± 50 ms around granule cell excitation.

When the $\alpha 1$ receptor-mediated current was turned off, the effects were smaller and resonance was restricted over about ± 10 ms. Interestingly, time-related firing parameters (time window, time to first spike, first spike standard deviation) showed much sharper tuning than tonic firing (number of spikes). Moreover, tuning of time-related parameters decreased with E/I along with the decreasing inhibitory control, while GABA leakage did not alter the dynamics of inhibition substantially.

The model also predicted how VDCC and NMDA currents would be regulated by $\alpha 1$ and $\alpha 6$ receptors. VDCC current regulation strictly followed the number of spikes, as these channels open during the upstroke (D'Angelo et al., 1997, 2001; Gandolfi et al., 2014). The $\alpha 6$ receptor-mediated regulation of the NMDA current showed a broad tuning extending over ± 50 ms and reflecting the slow NMDA current kinetics (D'Angelo et al., 1995; Schwartz et al., 2012). Puzzlingly, the effect of inhibition on the NMDA current showed a precession with E/I (from -20 to $+30$ ms phase-lag) suggesting a complex voltage-dependent interaction between NMDA channel unblock, depolarization and inhibitory control.

IMPLICATIONS FOR DYNAMIC INHIBITORY CONTROL DURING CIRCUIT ACTIVITY

The dynamic control of inhibition by $\alpha 6$ and $\alpha 1$ receptors could have specific consequences during local microcircuit activation. *Feed-forward* inhibition affects granule cell excitation around 5 ms after mossy fiber activation (D'Angelo and De Zeeuw, 2009). With 5 ms phase-lag, the model predicted a higher impact for $\alpha 6$ mediated inhibition (except for the number of spikes at low E/I , where $\alpha 6$ and $\alpha 1$ affected the response in a similar way). *Feed-back* inhibition occurs after about 10 ms. With 10 ms phase-lag, the overall effect was also dominated by $\alpha 6$ mediated inhibition, but $\alpha 1$ and $\alpha 6$ effects were similar for time-to-first spike and first-spike standard deviation (and also on the number of spikes at low E/I). Therefore, in summary, the $\alpha 6$ component dominated on feed-forward inhibition, while the $\alpha 1$ component gained relevance in controlling the timing of granule cell output firing at low E/I during feed-back inhibition. Interestingly, during feedback inhibition at low E/I the $\alpha 1$ component is often more effective than the $\alpha 6$ component. Concerning the NMDA current, phase-lag precession suggested that the maximum impact of $\alpha 6$ mediated inhibition at 5–10 ms phase-lag was also achieved at low E/I . The multiple combinations of these effects and the complex inhibitory patterns provided by $\alpha 1$ and $\alpha 6$ subunit-containing GABA-A receptors make phasic inhibition particularly suitable to finely regulate the delay and precision of granule cell firing.

These properties may have an impact on spike-timing dependent plasticity (STDP) induction and on its interaction with low-frequency coherent oscillations reported in the cerebellar granular layer (Pellerin and Lamarre, 1997; Hartmann and Bower, 1998) and deserve future experimental assessment.

CONSIDERATIONS ON INHIBITORY CONTROL OF INFORMATION TRANSFER

The extensive simulation strategy adopted in this paper suggests how phasic inhibition provided by Golgi cells controls information transfer through the granular layer. For each E/I value, release

probabilities generated a complex subspace, such that similar firing parameter values could be found with different E/I and pE/pI combinations with a redundancy of $80 \div 90\%$ ($CF = 0.1 \div 0.2$) (Borst and Theunissen, 1999; Sadeghi et al., 2007; Ince et al., 2009). The actual number of excitatory synapses may be relatively unimportant, provided that the number of inhibitory synapses is properly set, suggesting that the granular layer has intrinsic re-scaling properties with respect to the intensity of the inputs. Synaptic plasticity, mostly through pE , could allow to select points in this computational landscape for any specific E/I and pE/pI combination.

The amount of transmitted information (MI ; Borst and Theunissen, 1999; Sadeghi et al., 2007; Ince et al., 2009), depends on the signal-to-noise (S/N) ratio. Since short bursts (1–3 spikes: see **Figure 4B**) at the mossy fiber—granule cell synapse carry the largest fraction of MI (Arleo et al., 2010), it is expected that regulation of first-spike delay and precision by phasic inhibition contributes substantially to regulate MI transfer through the cerebellum input stage (Garrido et al., 2013). It should also be noted that quantal fluctuations in GABA release generate synaptic noise, which should be smaller the larger the number of active synapses and the higher their release probabilities. Therefore, redundant E/I and pE/pI combinations giving same granule cell output patterns may not be equivalent in terms of MI transfer.

THE FIVE REASONS WHY PHASIC INHIBITION IS NEEDED FOR DYNAMIC CONTROL

In summary, simulations identify five main reasons why phasic inhibition is needed for dynamic control of spike transmission at the mossy fiber—granule cell relay. (1) During burst transmission, tonic inhibition simply scales the effect of phasic inhibition on tonic spike discharge (*number of spikes*) without affecting time-related parameters (time to first spike and time window) significantly. (2) During inhibition with variable E/I phase, the pattern observed during bursts is reversed, so that phasic inhibition specifically affects time-related parameters without affecting tonic spike discharge significantly. (3) During inhibition with variable E/I phase, tonic GABA leakage does not alter the dynamics of inhibition substantially, so that tonic inhibition simply scales the effect of phasic inhibition on firing parameters. (4) The differential kinetics imposed by $\alpha 1$ and $\alpha 6$ receptors during inhibition with bursts or with variable E/I phase may not be explained by tonic inhibitory effects. (5) Phasic inhibition reduced redundancy specifically for time-related parameters.

CONCLUSIONS

Biologically realistic simulations show that phasic inhibition, by exploiting the different kinetics of $\alpha 1$ and $\alpha 6$ receptor-mediated responses, can effectively regulate the delay and precision of granule cell firing. The effect of $\alpha 6$ receptors dominated during burst transmission while that of $\alpha 1$ receptors emerged during single-pulse transmission with variable phase lag, so that $\alpha 1$ and $\alpha 6$ receptors proved suitable for single-spike and burst control, respectively. These mechanisms in turn may regulate coincidence detection of calcium signals required for STDP and for its integration during theta-cycles (D'Angelo and De Zeeuw, 2009).

Conversely, no specific effects of tonic inhibition occurred beyond a proportionate scaling of granule cell discharge duration and frequency, compatible with a gain control mechanisms over tonic firing (Mitchell and Silver, 2003). Therefore, these model simulations imply that phasic inhibition endows the cerebellar cortex with a mechanism suitable for improving spatio-temporal reconfiguration of the mossy fiber input and for promoting dynamic signal processing in the cerebellar cortex (Marr, 1969; Eccles, 1973; Fujita, 1982). Critical tests to this prediction could be obtained by experiments, in which multiple different mossy fiber and Golgi cell axon fibers are activated independently with arbitrary phases. Although this protocol would be impractical with current electrophysiology, it may become at hand by combining recently developed imaging and optogenetic techniques (e.g., see Gandolfi et al., 2014).

ACKNOWLEDGMENTS

We thank Leda Roggeri for technical assistance. This work was supported by European Union grants to Egidio D'Angelo [CEREBNET FP7-ITN238686, REALNET FP7-ICT270434, Human Brain Project (HBP-604102)].

REFERENCES

- Arenz, A., Silver, R. A., Schaefer, A. T., and Margrie, T. W. (2008). The contribution of single synapses to sensory representation *in vivo*. *Science* 321, 977–980. doi: 10.1126/science.1158391
- Arleo, A., Nieus, T., Bezzi, M., D'Errico, A., D'Angelo, E., and Coenen, O. J. (2010). How synaptic release probability shapes neuronal transmission: information-theoretic analysis in a cerebellar granule cell. *Neural Comput.* 22, 2031–2058. doi: 10.1162/NECO_a_00006-Arleo
- Armano, S., Rossi, P., Taglietti, V., and D'Angelo, E. (2000). Long-term potentiation of intrinsic excitability at the mossy fiber-granule cell synapse of rat cerebellum. *J. Neurosci.* 20, 5208–5216.
- Barberis, A., Cherubini, E., and Mozrzymas, J. W. (2000). Zinc inhibits miniature GABAergic currents by allosteric modulation of GABAA receptor gating. *J. Neurosci.* 20, 8618–8627.
- Borst, A., and Theunissen, F. E. (1999). Information theory and neural coding. *Nat. Neurosci.* 2, 947–957. doi: 10.1038/14731
- Brandalise, F., Mapelli, L., Gerber, U., and Rossi, P. (2012). Golgi cell-mediated activation of postsynaptic GABA(B) receptors induces disinhibition of the Golgi cell-granule cell synapse in rat cerebellum. *PLoS ONE* 7:e43417. doi: 10.1371/journal.pone.0043417
- Brickley, S. G., Cull-Candy, S. G., and Farrant, M. (1996). Development of a tonic form of synaptic inhibition in rat cerebellar granule cells resulting from persistent activation of GABAA receptors. *J. Physiol.* 497(Pt 3), 753–759.
- Brickley, S. G., Revilla, V., Cull-Candy, S. G., Wisden, W., and Farrant, M. (2001). Adaptive regulation of neuronal excitability by a voltage-independent potassium conductance. *Nature* 409, 88–92. doi: 10.1038/35051086
- Cesana, E., Pietrajtis, K., Bidoret, C., Isope, P., D'Angelo, E., Dieudonné, S., et al. (2013). Granule cell ascending axon excitatory synapses onto Golgi cells implement a potent feedback circuit in the cerebellar granular layer. *J. Neurosci.* 33, 12430–12446. doi: 10.1523/JNEUROSCI.4897-11.2013
- Chadderton, P., Margrie, T. W., and Häusser, M. (2004). Integration of quanta in cerebellar granule cells during sensory processing. *Nature* 428, 856–860. doi: 10.1038/nature02442
- Cherubini, E., and Conti, F. (2001). Generating diversity at GABAergic synapses. *Trends Neurosci.* 24, 155–162. doi: 10.1016/S0166-2236(00)01724-0
- D'Angelo, E., De Filippi, G., Rossi, P., and Taglietti, V. (1995). Synaptic excitation of individual rat cerebellar granule cells *in situ*: evidence for the role of NMDA receptors. *J. Physiol.* 484(Pt 2), 397–413.
- D'Angelo, E., De Filippi, G., Rossi, P., and Taglietti, V. (1997). Synaptic activation of Ca²⁺ action potentials in immature rat cerebellar granule cells *in situ*. *J. Neurophysiol.* 78, 1631–1642.

- D'Angelo, E., and De Zeeuw, C. I. (2009). Timing and plasticity in the cerebellum: focus on the granular layer. *Trends Neurosci.* 32, 30–40. doi: 10.1016/j.tins.2008.09.007
- D'Angelo, E., Nieuws, T., Maffei, A., Armano, S., Rossi, P., Taglietti, V., et al. (2001). Theta-frequency bursting and resonance in cerebellar granule cells: experimental evidence and modeling of a slow k^+ -dependent mechanism. *J. Neurosci.* 21, 759–770.
- D'Angelo, E., Rossi, P., Armano, S., and Taglietti, V. (1999). Evidence for NMDA and mGlu receptor-dependent long-term potentiation of mossy fiber-granule cell transmission in rat cerebellum. *J. Neurophysiol.* 81, 277–287.
- D'Angelo, E., Rossi, P., and Taglietti, V. (1993). Different proportions of *N*-methyl-D-aspartate and non-*N*-methyl-D-aspartate receptor currents at the mossy fibre-granule cell synapse of developing rat cerebellum. *Neuroscience* 53, 121–130. doi: 10.1016/0306-4522(93)90290-V
- D'Angelo, E., Solinas, S., Mapelli, J., Gandolfi, D., Mapelli, L., and Prestori, F. (2013). The cerebellar Golgi cell and spatiotemporal organization of granular layer activity. *Front. Neural Circuits* 7:93. doi: 10.3389/fncir.2013.00093
- D'Errico, A., Prestori, F., and D'Angelo, E. (2009). Differential induction of bidirectional long-term changes in neurotransmitter release by frequency-coded patterns at the cerebellar input. *J. Physiol.* 587, 5843–5857. doi: 10.1113/jphysiol.2009.177162
- Dieudonne, S. (1998). Submillisecond kinetics and low efficacy of parallel fibre-Golgi cell synaptic currents in the rat cerebellum. *J. Physiol.* 510(Pt 3), 845–866. doi: 10.1111/j.1469-7793.1998.845bj.x
- DiGregorio, D. A., Nusser, Z., and Silver, R. A. (2002). Spillover of glutamate onto synaptic AMPA receptors enhances fast transmission at a cerebellar synapse. *Neuron* 35, 521–533. doi: 10.1016/S0896-6273(02)00787-0
- Diwakar, S., Magistretti, J., Goldfarb, M., Naldi, G., and D'Angelo, E. (2009). Axonal Na^+ channels ensure fast spike activation and back-propagation in cerebellar granule cells. *J. Neurophysiol.* 101, 519–532. doi: 10.1152/jn.90382.2008
- Dugué, G. P., Brunel, N., Hakim, V., Schwartz, E., Chat, M., Lévesque, M., et al. (2009). Electrical coupling mediates tunable low-frequency oscillations and resonance in the cerebellar Golgi cell network. *Neuron* 61, 126–139. doi: 10.1016/j.neuron.2008.11.028
- Eccles, J. C. (1973). The cerebellum as a computer: patterns in space and time. *J. Physiol.* 229, 1–32.
- Eccles, J., Llinas, R., and Sasaki, K. (1964). Golgi cell inhibition in the cerebellar cortex. *Nature* 204, 1265–1266. doi: 10.1038/2041265a0
- Farrant, M., and Nusser, Z. (2005). Variations on an inhibitory theme: phasic and tonic activation of GABA(A) receptors. *Nat. Rev. Neurosci.* 6, 215–229. doi: 10.1038/nrn1625
- Forti, L., Cesana, E., Mapelli, J., and D'Angelo, E. (2006). Ionic mechanisms of autorhythmic firing in rat cerebellar Golgi cells. *J. Physiol.* 574, 711–729. doi: 10.1113/jphysiol.2006.110858
- Fujita, M. (1982). Adaptive filter model of the cerebellum. *Biol. Cybern.* 45, 195–206. doi: 10.1007/BF00336192
- Gandolfi, D., Lombardo, P., Mapelli, J., Solinas, S., and D'Angelo, E. (2013). Theta-frequency resonance at the cerebellum input stage improves spike timing on the millisecond time-scale. *Front. Neural Circuits* 7:64. doi: 10.3389/fncir.2013.00064
- Gandolfi, D., Pozzi, P., Tognolina, M., Chirico, G., Mapelli, J., and D'Angelo, E. (2014). The spatiotemporal organization of cerebellar network activity resolved by two-photon imaging of multiple single neurons. *Front. Cell. Neurosci.* 8:92. doi: 10.3389/fncel.2014.00092
- Garrido, J. A., Ros, E., and D'Angelo, E. (2013). Spike timing regulation on the millisecond scale by distributed synaptic plasticity at the cerebellum input stage: a simulation study. *Front. Comput. Neurosci.* 7:64. doi: 10.3389/fncom.2013.00064
- Glykys, J., and Mody, I. (2007). Activation of GABAA receptors: views from outside the synaptic cleft. *Neuron* 56, 763–770. doi: 10.1016/j.neuron.2007.11.002
- Griffen, T. C., and Maffei, A. (2014). GABAergic synapses: their plasticity and role in sensory cortex. *Front. Cell. Neurosci.* 8:91. doi: 10.3389/fncel.2014.00091
- Hadley, S. H., and Amin, J. (2007). Rat $\alpha 6\beta 2\delta$ GABAA receptors exhibit two distinct and separable agonist affinities. *J. Physiol.* 581, 1001–1018. doi: 10.1113/jphysiol.2007.132886
- Hamann, M., Rossi, D. J., and Attwell, D. (2002). Tonic and spillover inhibition of granule cells control information flow through cerebellar cortex. *Neuron* 33, 625–633. doi: 10.1016/S0896-6273(02)00593-7
- Hámori, J., and Somogyi, J. (1983). Differentiation of cerebellar mossy fiber synapses in the rat: a quantitative electron microscope study. *J. Comp. Neurol.* 220, 365–377. doi: 10.1002/cne.902200402
- Hartmann, M. J., and Bower, J. M. (1998). Oscillatory activity in the cerebellar hemispheres of unrestrained rats. *J. Neurophysiol.* 80, 1598–1604.
- Hines, M. L., and Carnevale, N. T. (2001). NEURON: a tool for neuroscientists. *Neuroscientist* 7, 123–135. doi: 10.1177/107385840100700207
- Hull, C., and Regehr, W. G. (2012). Identification of an inhibitory circuit that regulates cerebellar Golgi cell activity. *Neuron* 73, 149–158. doi: 10.1016/j.neuron.2011.10.030
- Ince, R. A., Petersen, R. S., Swan, D. C., and Panzeri, S. (2009). Python for information theoretic analysis of neural data. *Front. Neuroinform.* 3:4. doi: 10.3389/fninf.2009.11.004.2009
- Jakab, R. L., and Hámori, J. (1988). Quantitative morphology and synaptology of cerebellar glomeruli in the rat. *Anat. Embryol. (Berl.)* 179, 81–88. doi: 10.1007/BF00305102
- Jones, M. V., Jonas, P., Sahara, Y., and Westbrook, G. L. (2001). Microscopic kinetics and energetics distinguish GABA(A) receptor agonists from antagonists. *Biophys. J.* 81, 2660–2670. doi: 10.1016/S0006-3495(01)75909-7
- Kanichay, R. T., and Silver, R. A. (2008). Synaptic and cellular properties of the feedforward inhibitory circuit within the input layer of the cerebellar cortex. *J. Neurosci.* 28, 8955–8967. doi: 10.1523/JNEUROSCI.5469-07.2008
- Lamsa, K. P., Kullmann, D. M., and Woodin, M. A. (2010). Spike-timing dependent plasticity in inhibitory circuits. *Front. Synaptic Neurosci.* 2:8. doi: 10.3389/fnsyn.2010.00008
- Llinás, R., Urbano, F. J., Leznik, E., Ramírez, R. R., and van Marle, H. J. (2005). Rhythmic and dysrhythmic thalamocortical dynamics: GABA systems and the edge effect. *Trends Neurosci.* 28, 325–333. doi: 10.1016/j.tins.2005.04.006
- Maex, R., and De Schutter, E. (1998). Synchronization of golgi and granule cell firing in a detailed network model of the cerebellar granule cell layer. *J. Neurophysiol.* 80, 2521–2537.
- Mann, E. O., and Paulsen, O. (2007). Role of GABAergic inhibition in hippocampal network oscillations. *Trends Neurosci.* 30, 343–349. doi: 10.1016/j.tins.2007.05.003
- Mapelli, J., and D'Angelo, E. (2007). The spatial organization of long-term synaptic plasticity at the input stage of cerebellum. *J. Neurosci.* 27, 1285–1296. doi: 10.1523/JNEUROSCI.4873-06.2007
- Mapelli, J., Gandolfi, D., and D'Angelo, E. (2010a). Combinatorial responses controlled by synaptic inhibition in the cerebellum granular layer. *J. Neurophysiol.* 103, 250–261. doi: 10.1152/jn.00642.2009
- Mapelli, J., Gandolfi, D., and D'Angelo, E. (2010b). High-pass filtering and dynamic gain regulation enhance vertical bursts transmission along the mossy fiber pathway of cerebellum. *Front. Cell. Neurosci.* 4:14. doi: 10.3389/fncel.2010.00014
- Mapelli, L., Rossi, P., Nieuws, T., and D'Angelo, E. (2009). Tonic activation of GABAB receptors reduces release probability at inhibitory connections in the cerebellar glomerulus. *J. Neurophysiol.* 101, 3089–3099. doi: 10.1152/jn.91190.2008
- Mapelli, L., Solinas, S., and D'Angelo, E. (2014). Integration and regulation of glomerular inhibition in the cerebellar granular layer circuit. *Front. Cell. Neurosci.* 8:55. doi: 10.3389/fncel.2014.00055
- Marr, D. (1969). A theory of cerebellar cortex. *J. Physiol.* 202, 437–470.
- Mitchell, S. J., and Silver, R. A. (2003). Shunting inhibition modulates neuronal gain during synaptic excitation. *Neuron* 38, 433–445. doi: 10.1016/S0896-6273(03)00200-9
- Nielsen, T. A., DiGregorio, D. A., and Silver, R. A. (2004). Modulation of glutamate mobility reveals the mechanism underlying slow-rising AMPAR EPSCs and the diffusion coefficient in the synaptic cleft. *Neuron* 42, 757–771. doi: 10.1016/j.neuron.2004.04.003
- Nieuws, T., Sola, E., Mapelli, J., Saftenku, E., Rossi, P., and D'Angelo, E. (2006). LTP regulates burst initiation and frequency at mossy fiber-granule cell synapses of rat cerebellum: experimental observations and theoretical predictions. *J. Neurophysiol.* 95, 686–699. doi: 10.1152/jn.00696.2005
- Nusser, Z., and Mody, I. (2002). Selective modulation of tonic and phasic inhibitions in dentate gyrus granule cells. *J. Neurophysiol.* 87, 2624–2628. doi: 10.1152/jn.00866.2001
- Nusser, Z., Roberts, J. D., Baude, A., Richards, J. G., and Somogyi, P. (1995). Relative densities of synaptic and extrasynaptic GABAA receptors on cerebellar granule cells as determined by a quantitative immunogold method. *J. Neurosci.* 15, 2948–2960.

- Nusser, Z., Sieghart, W., and Somogyi, P. (1998). Segregation of different GABA_A receptors to synaptic and extrasynaptic membranes of cerebellar granule cells. *J. Neurosci.* 18, 1693–1703.
- Pellerin, J. P., and Lamarre, Y. (1997). Local field potential oscillations in primate cerebellar cortex during voluntary movement. *J. Neurophysiol.* 78, 3502–3507.
- Petrini, E. M., Nieus, T., Ravasenga, T., Succol, F., Guazzi, S., Benfenati, F., et al. (2011). Influence of GABA_AR monoliganded states on GABAergic responses. *J. Neurosci.* 31, 1752–1761. doi: 10.1523/JNEUROSCI.1453-10.2011
- Pugh, J. R., and Raman, I. M. (2005). GABA_A receptor kinetics in the cerebellar nuclei: evidence for detection of transmitter from distant release sites. *Biophys. J.* 88, 1740–1754. doi: 10.1529/biophysj.104.055814
- Rancz, E. A., Ishikawa, T., Duguid, I., Chadderton, P., Mahon, S., and Häusser, M. (2007). High-fidelity transmission of sensory information by single cerebellar mossy fibre boutons. *Nature* 450, 1245–1248. doi: 10.1038/nature05995
- Rossi, D. J., and Hamann, M. (1998). Spillover-mediated transmission at inhibitory synapses promoted by high affinity alpha6 subunit GABA(A) receptors and glomerular geometry. *Neuron* 20, 783–795. doi: 10.1016/S0896-6273(00)81016-8
- Rossi, D. J., Hamann, M., and Attwell, D. (2003). Multiple modes of GABAergic inhibition of rat cerebellar granule cells. *J. Physiol.* 548, 97–110. doi: 10.1113/jphysiol.2002.036459
- Rossi, P., D'Angelo, E., Magistretti, J., Toselli, M., and Taglietti, V. (1994). Age-dependent expression of high-voltage activated calcium currents during cerebellar granule cell development in situ. *Pflugers Arch.* 429, 107–116. doi: 10.1007/BF02584036
- Rossi, P., Mapelli, L., Roggeri, L., Gall, D., de Kerchove d'Exaerde, A., Schiffmann, S. N., et al. (2006). Inhibition of constitutive inward rectifier currents in cerebellar granule cells by pharmacological and synaptic activation of GABA receptors. *Eur. J. Neurosci.* 24, 419–432. doi: 10.1111/j.1460-9568.2006.04914.x
- Sadeghi, S. G., Chacron, M. J., Taylor, M. C., and Cullen, K. E. (2007). Neural variability, detection thresholds, and information transmission in the vestibular system. *J. Neurosci.* 27, 771–781. doi: 10.1523/JNEUROSCI.4690-06.2007
- Saviane, C., and Silver, R. A. (2007). Estimation of quantal parameters with multiple-probability fluctuation analysis. *Methods Mol. Biol.* 403, 303–317. doi: 10.1007/978-1-59745-529-9_19
- Schwartz, E. J., Rothman, J. S., Dugué, G. P., Diana, M., Rousseau, C., Silver, R. A., et al. (2012). NMDA receptors with incomplete Mg²⁺ block enable low-frequency transmission through the cerebellar cortex. *J. Neurosci.* 32, 6878–6893. doi: 10.1523/JNEUROSCI.5736-11.2012
- Silver, R. A., Traynelis, S. F., and Cull-Candy, S. G. (1992). Rapid-time-course miniature and evoked excitatory currents at cerebellar synapses in situ. *Nature* 355, 163–166. doi: 10.1038/355163a0
- Sola, E., Prestori, F., Rossi, P., Taglietti, V., and D'Angelo, E. (2004). Increased neurotransmitter release during long-term potentiation at mossy fibre-granule cell synapses in rat cerebellum. *J. Physiol.* 557, 843–861. doi: 10.1113/jphysiol.2003.060285
- Solinas, S., Forti, L., Cesana, E., Mapelli, J., De Schutter, E., and D'Angelo, E. (2007a). Computational reconstruction of pacemaking and intrinsic electroresponsiveness in cerebellar Golgi cells. *Front. Cell. Neurosci.* 1:2. doi: 10.3389/fncel.2007.03.002.2007
- Solinas, S., Forti, L., Cesana, E., Mapelli, J., De Schutter, E., and D'Angelo, E. (2007b). Fast-reset of pacemaking and theta-frequency resonance patterns in cerebellar golgi cells: simulations of their impact *in vivo*. *Front. Cell. Neurosci.* 1:4. doi: 10.3389/fncel.2007.03.004.2007
- Solinas, S., Nieus, T., and D'Angelo, E. (2010). A realistic large-scale model of the cerebellum granular layer predicts circuit spatio-temporal filtering properties. *Front. Cell. Neurosci.* 4:12. doi: 10.3389/fncel.2010.00012
- Tia, S., Wang, J. F., Kotchabhakdi, N., and Vicini, S. (1996). Distinct deactivation and desensitization kinetics of recombinant GABA_A receptors. *Neuropharmacology* 35, 1375–1382. doi: 10.1016/S0028-3908(96)00018-4
- Timmann, D., Watts, S., and Hore, J. (1999). Failure of cerebellar patients to time finger opening precisely causes ball high-low inaccuracy in overarm throws. *J. Neurophysiol.* 82, 103–114.
- Vos, B. P., Volny-Luraghi, A., and De Schutter, E. (1999). Cerebellar Golgi cells in the rat: receptive fields and timing of responses to facial stimulation. *Eur. J. Neurosci.* 11, 2621–2634. doi: 10.1046/j.1460-9568.1999.00678.x
- Wall, M. J. (2002). Furosemide reveals heterogeneous GABA(A) receptor expression at adult rat Golgi cell to granule cell synapses. *Neuropharmacology* 43, 737–749. doi: 10.1016/S0028-3908(02)00085-0
- Wenner, P. (2011). Mechanisms of GABAergic homeostatic plasticity. *Neural Plast.* 2011, 489470. doi: 10.1155/2011/489470

Conflict of Interest Statement: The authors declare that the research was conducted in the absence of any commercial or financial relationships that could be construed as a potential conflict of interest.

Received: 18 June 2014; accepted: 04 August 2014; published online: 25 August 2014.

Citation: Nieus TR, Mapelli L and D'Angelo E (2014) Regulation of output spike patterns by phasic inhibition in cerebellar granule cells. *Front. Cell. Neurosci.* 8:246. doi: 10.3389/fncel.2014.00246

This article was submitted to the journal *Frontiers in Cellular Neuroscience*.

Copyright © 2014 Nieus, Mapelli and D'Angelo. This is an open-access article distributed under the terms of the Creative Commons Attribution License (CC BY). The use, distribution or reproduction in other forums is permitted, provided the original author(s) or licensor are credited and that the original publication in this journal is cited, in accordance with accepted academic practice. No use, distribution or reproduction is permitted which does not comply with these terms.